Scandium in aluminium alloys

J. Røyset* and N. Ryum

A considerable part of the available literature on scandium in aluminium alloys is reviewed. Experimental data and assessments of the binary Al–Sc phase diagram, a wide range of ternary Al–Sc–X phase diagrams and a few higher order phase diagrams are accounted for, with emphasis on the aluminium rich part of the diagrams. The phase which is in equilibrium with Al, Al_3Sc, can form by several different mechanisms, all of which are described. The precipitation kinetics of Al_3Sc in binary Al–Sc alloys are discussed, and an overview of the reported influences of ternary alloying elements on the precipitation of Al_3Sc is given. The Al_3Sc phase particles can serve as a grain refiner in the Al melt, a dispersoid for controlling the grain structure of the alloy and a strengthening precipitate. Several examples of these three effects are mentioned, both in binary Al–Sc alloys, and in more complex alloys. The reported effects of Sc on the precipitation behaviour in Al–Cu, Al–Mg–Si, Al–Zn–Mg and Al–Li alloys are also revised. A brief account of the effects of Sc additions on the corrosion behaviour of Al and Al-alloys is given. Finally, some views on the current and future use of Sc-containing Al alloys are given.

Keywords: Al–Sc, Phase diagrams, Grain refinement, Precipitation, Dispersoids IMR/421

Some trivia about scandium

Scandium is element no. 21 in the periodic system. It is a light metal, with density $\rho \approx 3$ g cm^{-3}, and melting point 1541°C.[1] This is in itself an attractive combination of properties for special purposes, but owing to limited availability and high price, scandium metal has virtually no applications at the present time. Some of the areas where scandium is used as an additive or dopant, are

(i) Addition as metal and iodide to high intensity halide lamps to make the emitted light spectrum resemble that of sunlight
(ii) Dopant in garnets for lasers
(iii) Alloying element in aluminium alloys.

Scandium and yttrium bear many resemblances to the lanthanides (the elements 57 through 71 in the periodic table). In the technical literature, the term 'rare earth metals' (R.E.M.) sometimes means only the lanthanides and sometimes scandium, yttrium and the lanthanides. Throughout this paper, the latter definition is used. As can be seen in Fig. 1, Sc is located close to Ti, Y and Zr in the periodic table, and with respect to interactions with aluminium there are quite a few resemblances between these four elements.

Binary aluminium–scandium system

Al–Sc phase diagram

Apparently, the first publication of the complete Al–Sc phase diagram in English was by Russian scientists at an international conference in the USA in 1964 (Fig. 2).[2] The same diagram appears in English translations of two Russian journals a year later,[3,4] and the phase diagram of these three publications is reproduced in various phase diagram handbooks.[5,6] With small exceptions, the invariant points from this early investigation have been preserved in phase diagram assessments until recently.[7–10]

As one can see, the two elements form four equilibrium intermetallic phases: Al_3Sc, Al_2Sc, AlSc and $AlSc_2$. The phase which is in thermodynamic equilibrium with Al is Al_3Sc. In the early work,[2–4] it was concluded that there was a peritectic reaction

$$\text{Liq.} + Al_3Sc = \alpha(Al)$$

occurring at 665°C. Later studies[11–14] have shown that Al and Al_3Sc form eutectically from the melt

$$\text{Liq.} = \alpha(Al) + Al_3Sc$$

In spite of this, the peritectic temperature of the early work[2–4] has occasionally been used in assessing the Al–Sc phase diagram.[7,15]

In the early work,[2–4] it was found that the Al_3Sc and $AlSc_2$ phases form peritectically at approx. 1320 and 1195°C, respectively, whereas the Al_2Sc and AlSc phases were found to form congruently from the melt at approx. 1420 and 1300°C, respectively. It was also found[2–4] that Al_2Sc and AlSc form a eutectic at approx. 1150°C, and that $AlSc_2$ and Sc form a eutectic at approx. 945°C. In a later assesment,[9] it is argued that the $AlSc_2$ phase should be expected to melt congruently rather than peritectically.

The phase diagram of Refs 2–4 indicates a melting point of Sc of 1535°C and a transition temperature of

Department of Materials Technology, Norwegian University of Science and Technology, N-7491 Trondheim, Norway

*Corresponding author. Present address: Hydro Aluminium, R&D Sunndal, PO Box 219, N-6601 Sunndalsøra, Norway, email Jostein.Royset@hydro.com

Published by Maney for the Institute and ASM International
DOI 10.1179/174328005X14311

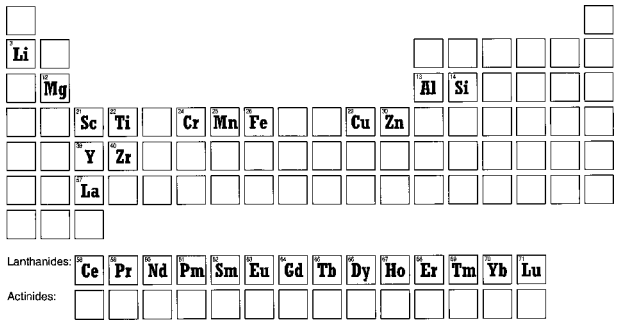

1 Periodic table of elements with Al, main alloying elements in Al-alloys and rare earth elements

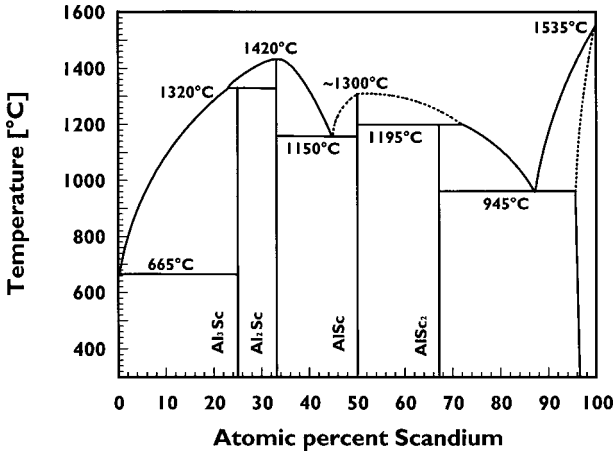

2 Sketch of first reported Al–Sc phase diagram[2–4]

α-Sc to β-Sc of 1350°C. In the phase diagram assessment of Ref. 8, these temperature are adjusted to 1541 and 1337°C, respectively.

A recent experimental investigation of selected compositions in the Al–Sc phase diagram[16,17] deviates significantly from the early work.[2–4] Most of the determined invariant temperatures are different. It is also found that the $AlSc_2$ phase melts congruently, as suggested previously,[9] and at a temperature of approx. 1300°C. The most prominent difference, however, is the finding of an extensive solid solubility of Al in β-Sc and a eutectoid transformation

$$\beta\text{-Sc} = AlSc_2 + \alpha\text{-Sc}$$

occurring at approx. 970°C. A sketch of the complete phase diagram based on these new findings[16] is shown in Fig. 3.

The four intermetallic phases are drawn as stoichiometric line-compounds in all the published phase diagrams. However, it has been suggested[16] that the AlSc phase is slightly off-stoichiometric and that it has a composition range of approximately 52–54%Sc.

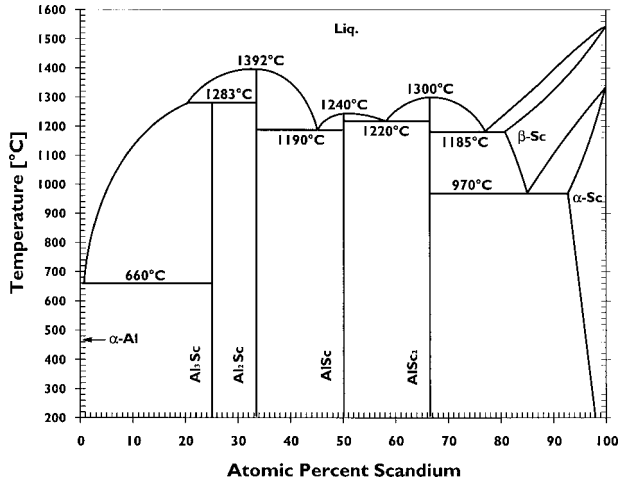

3 Sketch of Al–Sc binary phase diagram; eutectic temperature of $Al + Al_3Sc$ is adapted from Ref. 10; peritectic temperature of Al_3Sc and temperature of congruent melting of Al_2Sc are calculated in Ref. 16; all other binary invariant points are reported experimental values in Ref. 16

Microstructural observations[18] indicate that the Al_3Sc phase also has a solubility range. An overview of the different phases in the Al–Sc system is given in Table 1.[8] Reported enthalpies of formation for the intermetallic phases are given in Table 2. There is a considerable difference in the data reported in Refs 16 and 19. A comparison between the two data sets as well as with other works (not included in the present review) done in Ref. 16 shows that the data of Ref. 16 are more in line with other reported results.

Al rich side of Al–Sc phase diagram

As for the eutectic reaction

$$\text{Liq.} = \alpha(\text{Al}) + Al_3Sc$$

the reported eutectic temperature varies between 655 and 659°C.[11–14,22,23] The eutectic composition is approx. 0·6 wt-%,[11,14] and the solid solubility of Sc in Al at the eutectic temperature is approx. 0·35 wt-%.[12]

Table 2 Some reported enthalpies of formation [kJ mol^{-1}] for intermetallic phases in Al–Sc system

Reference	Enthalpy	Al_3Sc	Al_2Sc	AlSc	$AlSc_2$
19	$-\Delta H^0_{298}$	239·5	282·4	124·0	84·7
20	$-\Delta H^0_0$*	193			
16	$-\Delta H^0_{300}$	174	142	91·8	110
21	$-\Delta H^0_0$*	180			

*Calculated.

Table 1 Overview of phases in Al–Sc system[8]

Phase	Pearson symbol	Space group	Strukturbericht designation	Prototype	Lattice parameter, Å	Density, g cm^{-3}
Al	cF4	$Fm\bar{3}m$	A1	Cu	a=4·0496	2·699
Al_3Sc	cP4	$Pm\bar{3}m$	$L1_2$	$AuCu_3$	a=4·103	3·026
Al_2Sc	cF24	$Fd\bar{3}m$	C15	Cu_2Mg	a=7·582	3·015
AlSc	cP2	$Pm\bar{3}m$	B2	CsCl	a=3·450	2·909
$AlSc_2$	hP6	$P6_3/mmc$	$B8_2$	Ni_2In	a=4·888 c=6·166	3·043
β-Sc	cI2	$Im\bar{3}m$	A2	W	a=3·73 (estimated)	2·880 (estimated)
α-Sc	hP2	$P6_3/mmc$	A3	Mg	a=3·3088 c=5·2680	2·9890

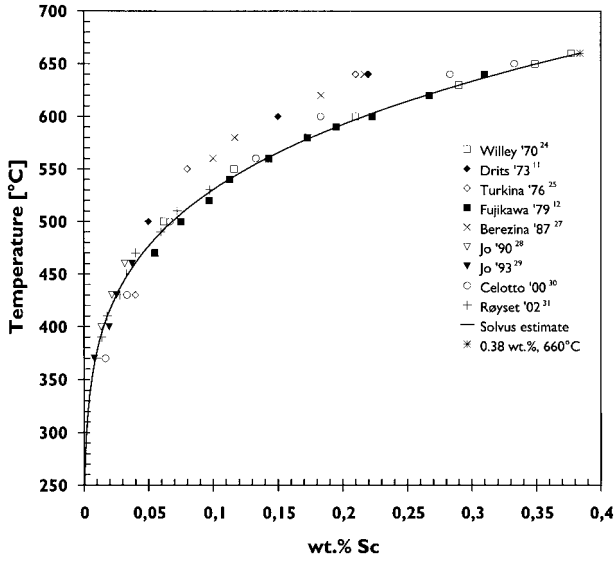

4 Reported values of Al solvus line in Al–Sc phase diagram: full line is solvus estimate assuming regular solution, and applying maximum solubility as assessed in Ref. 10 and experimental data of Ref. 31

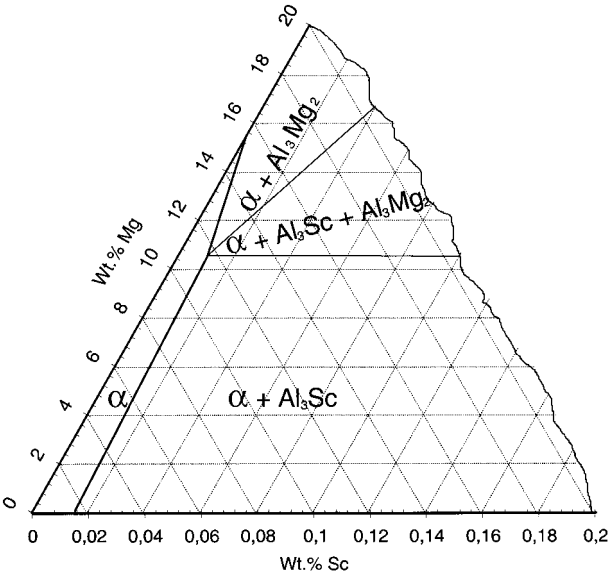

5 Isothermal section of Al-corner of Al–Mg–Sc phase diagram at 430°C: redrawn from Ref. 25

The solvus line of Sc in Al has been estimated by several researchers and over a wide temperature range.[11,12,24–31] All the reported measurements are summarised in Fig. 4. There is some spread in the results, most noticeably between data from Russian and non-Russian papers.

In most practical cases, solidification of alloys occurs under non-equilibrium conditions. Thus, the final microstructure might be different from what the equilibrium phase diagram predicts. In the case of dilute Al–Sc alloys, this is illustrated in a metastable state diagram for solidification at a cooling rate of approx. 100 K s^{-1}.[32] The temperature of the eutectic reaction decreases by 3–4°C, and the eutectic composition increases from approx. 0·6 wt-% to approx. 0·7 wt-%. Also, the maximum solid solubility of Sc in Al increases to approx. 0·6 wt-%.[32]

Ternary, quaternary and higher order Al–Sc–X(–X_2–X_3–...) phase diagrams

A wide range of ternary, quaternary and higher order Al–Sc–X(–X_2–X_3–…) phase diagrams has been reported in the literature, the majority in Russian journals. Some of the Russian journals do not have parallel English translations, and thus these data are less accessible for the non-Russian reader. However, a good overview of the majority of the published material is available.[33] Not all of the published phase diagrams comprise the full composition ranges. In the present review, the emphasis is placed on phase diagrams of Al–Sc with elements that are technologically important alloying elements with aluminium.

Ternary phase diagrams with precipitate-forming elements

Al–Mg–Sc

The Al–Mg–Sc phase diagram seems to be the Al–Sc–X diagram that is best described in the technical literature. In an investigation of Al–Mg–Sc alloys with up to 26 wt-%Mg and 3 wt-%Sc[25] a ternary eutectic

$$\text{Liq.} = \alpha - \text{Al} + \text{Al}_3\text{Mg}_2 + \text{Al}_3\text{Sc}$$

was observed at 447°C. Two vertical cross-sections and one isothermal section at 430°C of the phase diagram were constructed (Fig. 5). It was found that Mg and Sc mutually reduce each other's solid solubility in Al. The 'corner' of the α-Al field was determined to be at 10·5 wt-%Mg and 0·007 wt-%Sc at 430°C. No ternary AlMgSc phases were observed.

In another investigation, a vertical cross-section of the Al rich corner at a constant Sc level of 0·3 wt-% was constructed.[34] No ternary phases were reported. This phase diagram suggests, probably as a result of a lapse by the authors, that 0·3 wt-%Sc is a hypereutectic composition in binary Al–Sc.

Odinaev and co-workers explored the Al–Mg–Sc system for the whole Al–Mg range and for Sc contents up to 33·3 at.-%Sc.[35,36] An isothermal section at 400°C[35] was constructed. No ternary phases were observed in the region examined. A liquidus surface and three quasibinary cross-sections were also constructed.[36] Three quasibinary eutectics, three ternary eutectics and one ternary peritectic were observed in the examined composition range. The temperature for the eutectic reaction shown above was determined to be 435°C, and the composition was found to be 62·5 at.-%Al, 36·6 at.-%Mg and 0·9 at.-%Sc.

In a recent study,[37] the isothermal cross-section at 350°C was determined experimentally in the region delimited by the phases Al_3Mg_2, Al_3Sc, $AlSc_2$, MgSc, and Mg, meaning that the Al- and Sc-corners of the phase diagram were not explored. There are some discrepancies between the phase relations found in this work[37] and those found by Odinaev *et al.*[35] However, no ternary AlMgSc phases were found in Ref. 37 either. All the four intermetallic (Al,Sc) phases were found to dissolve a few percent Mg, seemingly by substituting Al. For Al_3Sc, this observation is sustained by other measurements[38] where some Mg content in Al_3Sc precipitates was found by three-dimensional atom probe microscopy. In Ref. 37, a calculated liquidus surface and

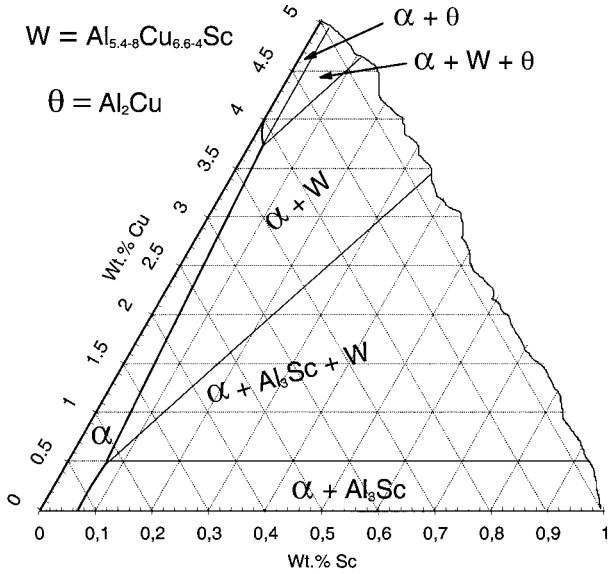

6 Isothermal section of Al-corner of Al–Cu–Sc phase diagram at 500°C: redrawn from Ref. 43

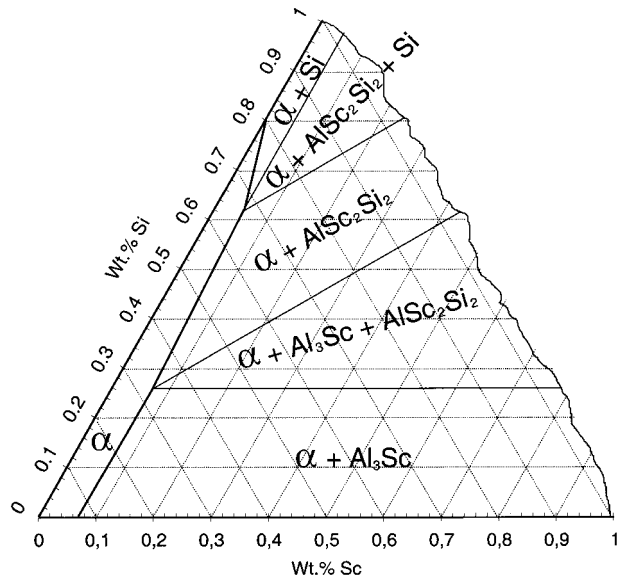

7 Isothermal section of Al-corner of Al–Sc–Si phase diagram at 500°C: redrawn from Ref. 33

several calculated vertical and isothermal cross-sections are also presented. Additional phase diagram calculations are reported in a separate paper.[39]

The phase relations in a diffusion couple between Al–1·77 wt-%Sc and pure Mg at 430°C have also been studied.[40] No ternary phases were reported, and the α-Al was found to be in equilibrium with Al_3Sc and Al_3Mg_2, in accordance with earlier work.[25,35,37] The maximum solid solubility of Mg and Sc in α-Al at this temperature was reported to be 15·27 at.-% (14 wt-%) and 0·33 at.-% (0·55 wt-%), respectively. Both these solubilities, and in particular that of Sc, is higher than what has been found earlier.[25] Considering the binary Al–Sc system, where the solubility of Sc in α-Al is only approx. 0·025 wt-% at 430°C, the high solubility of Sc reported in Ref. 40 for the ternary system is rather unlikely. It is possible that fine-scale Al_3Sc precipitates embedded in the α-Al matrix have been included in the electron probe analyses, and thus giving too high a value for the Sc content in solid solution.

Al–Cu–Sc

Two ternary phases, AlCuSc and $AlCu_2Sc$, were reported in an early investigation.[41] A later investigation of the Al-corner of the phase diagram[42] revealed that a ternary (Al,Cu,Sc) phase, named the 'W-phase', could be in thermodynamic equilibrium with α-Al. The following ternary invariant equilibria were found

$$\text{Liq.} + Al_3Sc = \alpha - Al + W(572^\circ C)$$

$$\text{Liq.} = \alpha - Al + Al_2Cu + W(546^\circ C)$$

Isothermal sections of the Al-corner at 450 and 500°C have been constructed[43] (Fig. 6). The solid solubility of Cu in Al was found to decrease somewhat with increasing Sc content, whereas the solid solubility of Sc in Al was not found to be influenced by the Cu content. The W-phase was suggested to be the compound $Al_{5·4–8}Cu_{6·6–4}Sc$.[43] A liquidus surface of the Al-corner has also been constructed.[44]

A more thorough review on the Al–Cu–Sc system is available in the literature.[45]

Al–Sc–Si

An isothermal section at 497°C has been constructed for the entire system.[46] A ternary phase, $AlSc_2Si_2$, was identified. This phase, frequently referred to as the 'V-phase', was found to be in thermodynamic equilibrium with Al_3Sc, Al, Si and ScSi at this temperature. A projection of the liquidus surface of the Al-corner has also been made.[47] Two ternary invariant reactions were reported

$$\text{Liq.} + Al_3Sc = \alpha - Al + V(617^\circ C)$$

$$\text{Liq.} = \alpha - Al + Si + V(574^\circ C)$$

Vertical cross-sections and isothermal sections of the Al-corner are reviewed in Ref. 33. The 550°C isothermal section is redrawn in Fig. 7. It seems that the solid solubility of Sc is not altered by an addition of Si, whereas the solubility of Si decreases somewhat with the Sc content.

Al–Sc–Zn

A sketch of a 'semi-isothermal' cross-section of the whole system, partially at 300°C and partially at 500°C, has been reported.[48] No ternary phases were found in this investigation. The phase relations in the Al rich range were found to be limited by the subsystem Al–Zn–Al_3Sc.

Another investigation of the subsystem Al–Zn–Al_2Sc confirmed that no ternary compounds are found in this composition range.[49] The liquidus surface was constructed. It is suggested that the section Zn–Al_2Sc is a quasibinary simple eutectic. A certain mutual solid solubility of Zn and Al_2Sc is indicated on the vertical cross-section, although no measurements of the compositions are presented. In addition to the quasibinary eutectic, one ternary peritectic and one ternary eutectic reaction was found. The ternary eutectic reaction

$$\text{Liq.} = \alpha - Al + Zn + Al_3Sc$$

was found to occur at 367°C.

Al–Li–Sc

An investigation of the phase relations in the Al-corner (up to 5 wt-%Li and 3 wt-%Sc) at 450°C revealed that

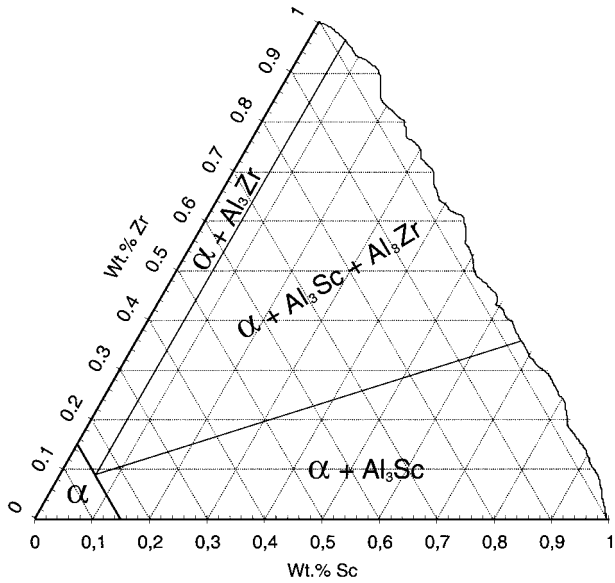

8 Isothermal section of Al-corner of Al–Sc–Zr phase diagram at 600°C: redrawn from Ref. 54

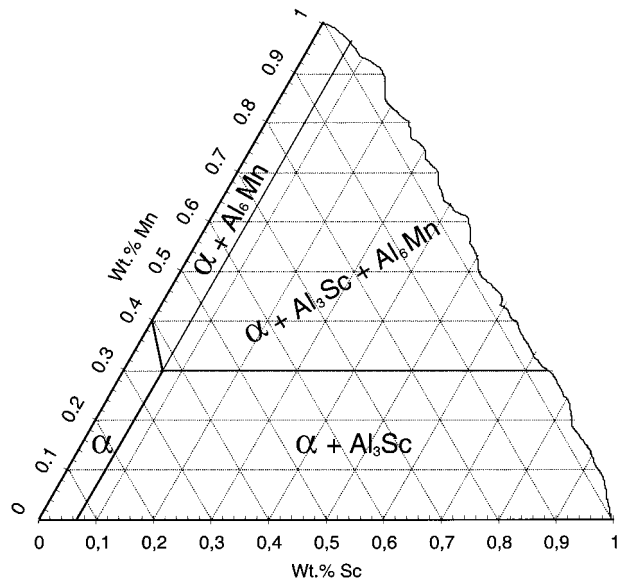

9 Isothermal section of Al-corner of Al–Mn–Sc phase diagram at 500°C: redrawn from Ref. 58

α-Al could be in equilibrium with either Al_3Sc or AlLi.[50] No ternary phases were observed. Thermal analyses indicated that the ternary eutectic reaction

$$\text{Liq.} = \alpha - \text{Al} + \text{Al}_3\text{Sc} + \text{AlLi}$$

occurs at approximately 595°C. It has been stated[47] that there are only minor mutual effects of Sc and Li on these elements' solid solubility in α-Al.

This statement is confirmed in another investigation,[51] where the Al–AlLi–AlSc subsystem is investigated. At 450°C, it is found that the AlLi phase can be in equilibrium with Al_3Sc, Al_2Sc and AlSc. No significant solubility of Li in Al_3Sc was observed. Several vertical cross-sections are constructed.

It should be noted that the existence of a ternary $Al_3(Li,Sc)$ phase has been reported,[52] which is in disagreement with the observations above.

Ternary phase diagrams with dispersoid-forming elements

Al–Sc–Zr

It has been shown[53] that at 600°C, the Al-corner consists of the phase fields α-Al + Al_3Sc, α-Al + Al_3Sc + Al_3Zr and α-Al + Al_3Zr. Further, it was discovered that there is a significant solid solubility of Zr in the Al_3Sc phase (approx. 35 wt-%) and some solid solubility of Sc in the Al_3Zr phase (approx. 5 wt-%). The lattice parameter of Al_3Sc was found to decrease when the phase dissolves Zr, and likewise the lattice parameter of the Al_3Zr was found to decrease when that phase dissolves Sc. For alloys in the α-Al + Al_3Sc phase field, the wt-%Zr/wt-%Sc ratio in the Al_3Sc particles was found to be approx. 2·2 times the wt-%Zr/wt-%Sc ratio of the alloy.[53] Isothermal sections of the Al-corner at 550 and 600°C are also constructed[54] (Fig. 8).

In another investigation,[55] two vertical cross-sections in the Al-corner were constructed, and a ternary peritectic reaction

$$\text{Liq.} + \text{Al}_3\text{Zr} = \alpha - \text{Al} + \text{Al}_3\text{Sc}$$

was found to take place at 659°C.

The 500°C isothermal section of the whole phase diagram has been investigated.[56] It is already known that Sc and Zr are completely miscible in the solid state. Here, it was also found that the compounds $AlSc_2$ and $AlZr_2$ are completely miscible. The extensions of the other single-phase fields are determined with various degrees of accuracy. The solubility of Zr in Al_3Sc was found to be 6 at.-% (approx. 16 wt-%), whereas the solubility of Sc in Al_3Zr was found to be 6·5 at.-% (approx. 7·3 wt-%). Contrary to Ref. 53, the lattice parameter of Al_3Sc was found to increase with increasing Zr content. The lattice parameter of Al_3Zr, however, was found to decrease with increasing Sc content, which is in accordance with the findings of Ref. 53.

The section Al_3Sc–Al_3Zr at 1200°C has recently been investigated.[57] The solubility of Sc in Al_3Zr was reported to be in the range 3–5 at.-% and the solubility of Zr in Al_3Sc was found to be 12·2 at.-%. In accordance with Ref. 53, the lattice parameters of Al_3Sc and Al_3Zr decrease with increasing content of Zr and Sc, respectively.

Al–Fe–Sc

The available data on this system is reviewed in Ref. 33, and an isothermal section at 500°C is reproduced. Three ternary Al–Fe–Sc phases are reported. The Al-corner of the isothermal section, however, seems to be limited by the subsystem Al–Al_3Sc–Al_3Fe, meaning that the α-Al cannot be in equilibrium with any of the ternary phases.

Al–Mn–Sc

The Al-corner of the phase diagram has been investigated.[58] No ternary phases were observed, meaning that in the solid state, only the Al_3Sc and the Al_6Mn phase can be in equilibrium with α-Al. An addition of Mn does not noticeably decrease the solid solubility of Sc, whereas an addition of Sc causes a distinct decrease in the solubility of Mn. Two isothermal sections were made, one at 500°C (Fig. 9) and one at 600°C. The 'corner' of the α-phase field was reported to be at 0·08 wt-%Sc and 0·2 wt-%Mn at 500°C and at 0·2 wt-%Sc and 0·55 wt-%Mn at 600°C.

Two vertical cross-sections were also constructed. A ternary eutectic

$$\text{Liq.} = \alpha\text{–Al} + \text{Al}_6\text{Mn} + \text{Al}_3\text{Sc}$$

at 649°C was identified. Several alloys in the section Al_3Sc–Al_6Mn have also been investigated,[59] and all were found to comprise a mixture of the two binary phases. Lattice parameter measurements of the Al_3Sc phase were interpreted as an indication of a slight solid solubility of Mn in Al_3Sc.

Al–Cr–Sc

Alloys in the composition range 30–100 at.-%Al have been studied[60] and an isothermal cross-section at 500°C was constructed. No ternary phases were identified. The phases that can be in equilibrium with the α-Al are thus Al_7Cr and Al_3Sc. The solubility of Cr in the Al_3Sc phase was found to be considerable, approximately 11 at.-%.

Other ternary Al–Sc–X phase diagrams

Al–Mo–Sc

An isothermal cross-section at 550°C has been constructed for the subsystem Al–Al_2Sc–Al_2Mo.[61] No ternary phases were reported. The phases in equilibrium with α-Al were found to be Al_3Sc and $Al_{12}Mo$.

Al–Sc–V

The section Al_3Sc–$Al_{21}V_2$ has been studied[62] and the vertical cross-section was constructed. No ternary phases were observed. Solid solubilities of V in the Al_3Sc phase of 1·4 at.-% and of Sc in $Al_{21}V_2$ of 2·5 at.-% are reported, although a considerably higher maximum solubility of V in Al_3Sc is suggested in the vertical cross-section. A quasibinary eutectic reaction

$$\text{Liq.} = \text{Al}_3\text{Sc} + \text{Al}_{21}\text{V}_2$$

is reported to occur at 917 K (644°C).

The section Al_3Sc–Al_3V at 1200°C has also been studied.[57] The solubilities of V in Al_3Sc and Sc in Al_3V are reported to be 2·7 and 0·7 at.-%, respectively. When V was dissolved in Al_3Sc, the lattice parameter of Al_3Sc was found to decrease.

Al–Sc–Ti

No ternary phase diagram is available. The section Al_3Sc–Al_3Ti at 1200°C has been studied.[57] A solubility of Ti in Al_3Sc of almost 12·5 at.-% was found, which corresponds to almost half of the Sc being substituted by Ti. The lattice parameter of Al_3Sc was found to decrease sharply with increasing Ti content. For the Al_3Ti phase, the solubility of Sc was found to be approx. 5 at.-%.

Al–Co–Sc

The ternary system for 0–70 at.-%Sc has been investigated.[63] Three ternary (Al,Co,Sc)-phases were identified. The only phases found to be in equilibrium with α-Al were the binary phases Al_3Sc and Al_9Co_2. An isothermal section at 600°C and the vertical cross-sections Al_3Sc–Al_9Co_2 and Al_3Sc–$Al_9Co_3Sc_2$ were constructed. The 'corner' of the α-phase field was reported in the text to be at 1·5 at.-%Co and 0·5 at.-%Sc, although in a table the numbers 0·2 at.-%Co and 0·1 at.-%Sc are reported. The solubilities of Co in the Al_3Sc phase and of Sc in the Al_9Co_2 phase were found to be 1·2 and $<0{\cdot}1$ at.-%, respectively. However, in the vertical cross-sections, it is suggested that the solubility of Co in Al_3Sc may be significantly higher at higher temperatures. The lattice parameter of Al_3Sc was not found to change with increasing Co content.

Al–Sc–Sr

The subsystem Al–Al_2Sc–Al_4Sr has been studied[64] and an isothermal section at 500°C was constructed. No ternary phases were detected, meaning that the phases in equilibrium with α-Al were found to be Al_3Sc and Al_4Sr. The solubility of Sc in Al_4Sr and of Sr in Al_3Sc was found to be low, typically less than 1·5–2 at.-%.

Al–Be–Sc

A study of the binary Be–Sc system and the ternary Al–Be–Sc system for up to 20 at.-%Sc (or 30 wt-%Sc) has been reported.[65] The 600°C isothermal section for the investigated ternary composition range was constructed. No ternary phases were observed. The α-Al can be in equilibrium with either Be, $Be_{13}Sc$ or Al_3Sc. It is suggested that the section Al–$Be_{13}Sc$ may be quasi-eutectic.

Al–Ba–Sc

An isothermal section at 500°C has been constructed.[66] No ternary phases were reported, and α-Al is in equilibrium with Al_4Ba and Al_3Sc. The solubility of Sc in Al_4Ba and of Ba in Al_3Sc was reported to be less than 2 at.-%.

Al–N–Sc

The region Al–AlN–ScN–Sc has been investigated.[67] A perovskite-type ternary phase, $AlN_{1-x}Sc_3$ was reported and an isothermal section at 1000°C was constructed. In the Al-corner, the Al melt was reported to be in equilibrium with AlN and Al_3Sc.

Quaternary and higher order Al–Sc–X–X_2(–X_3...) phase diagrams

Al–Mg–Sc–Zr

The published material is limited to investigations on Al rich alloys. A part of the liquidus surface of the 6 wt-%Mg section has been determined experimentally for the composition range 0–0·7 wt-%Sc and 0–0·4 wt-%Zr.[68] The 500°C isothermal phase relations in the Al-corner of the 6 wt-%Mg section has also been investigated,[69] for Sc and Zr concentrations of up to 3 wt-% and 4 wt-%, respectively. No ternary or quaternary phases were observed. Likewise the 430°C isothermal phase relations of the 4 at.-%Mg ($\sim$3·5 wt-%Mg) section have been investigated for up to 1·2 at.-%Sc (2 wt-%Sc) and up to 2·5 at.-%Zr (8 wt-%Zr).[70,71] No ternary or quaternary phases were observed in the present study either. The Al_3Sc phase was found to dissolve an amount of 12·2 at.-%Zr corresponding to a substitution of almost 50% of the Sc lattice positions, whereas the solubility of Sc in Al_3Zr was 4·4 at.-%, which corresponds to a substitution of almost 20% of the Zr lattice positions. Figure 4 in Refs 70 and 71 suggests that the Al content in the Al_3Zr-phase increases with increasing Sc content, however this is not substantiated in the text.

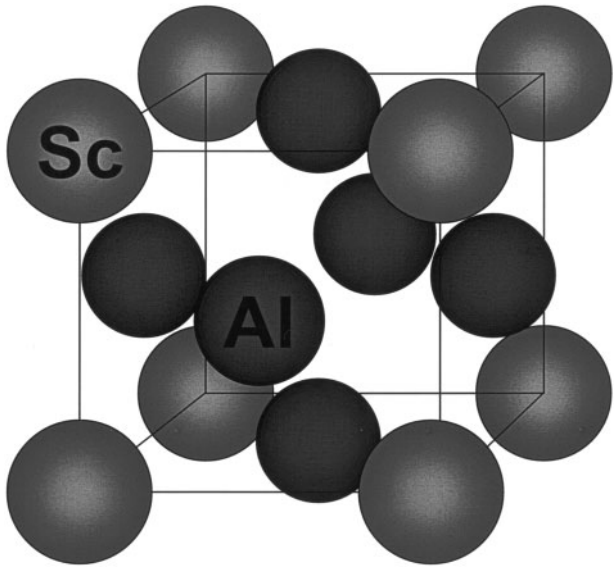

10 Atomic arrangement of Al_3Sc phase

Al–Mg–Sc–Ti–Zr

A vertical cross-section of the Al–Mg–Sc–Ti–Zr phase diagram for 0·3 wt-%Sc, 0·15 wt-%Ti, 0·15 wt-%Zr and 0–10 wt-%Mg has been constructed.[34] According to this diagram, the Al_3Zr phase is the first and Al_3Sc the last to form during solidification of the alloys. No ternary, quaternary or quinary phases are reported.

Al–Zn–Mg–Cu–Zr–Sc

A vertical cross-section of the full system as well as several sections of various sub-systems have been constructed.[72] For the full system, a section at 8 wt-% Zn, 2 wt-%Cu, 0·3 wt-%Zr and 0·3 wt-%Sc was constructed, where Mg varies from 0 to 8 wt-%. The only reported Sc-containing sub-system is that of Al–Zn–Mg–Cu–Sc. Here a vertical cross-section is constructed with the same levels of Zn, Cu and Sc as in the full system, whereas Mg varies from 0 to 6·5 wt-%.

No phases other than those known from the lower order systems were reported. Amongst the findings, it is interesting to note that in the solid state Al_3Sc is reported to be an equilibrium phase for all the investigated compositions. It is also interesting to note that the Sc-containing W-phase ($Al_{5·4–8}Cu_{6·6–4}Sc$, see the section on the Al–Cu–Sc ternary system) is an equilibrium phase at low Mg content and disappears as the Mg content increases.

Al–Li–Mg–Sc

The 400°C isothermal phase relations of the 0·2 wt-%Sc section have been investigated for the composition range 0–6 wt-%Mg and 0–5 wt-%Li.[73] The α-Al was found to be in equilibrium with AlLi, Al_2LiMg and Al_3Sc. No quaternary phases were observed. This investigation is also summarised in Ref. 50.

Al–Cu–Li–Sc

The aluminium rich corner of the system has been investigated for alloys with 0·6 wt-%Sc and with Cu and Li in the range 0–16 wt-% and 0–4 wt-%, respectively.[74] No quaternary phases were reported. Two sections of the phase diagram were constructed; a section of the 470°C isothermal tetrahedron at 0·6 wt-%Sc and a vertical section at 0·6 wt-%Sc and 2·6 wt-%Li. Two quaternary invariant equilibria were found, and the temperatures of the invariant points were estimated.

Al_3Sc phase

Rechkin and co-workers were, to the authors' knowledge, the first to publish a paper in an international journal identifying the Al_3Sc phase.[75] The phase was identified as cubic, with lattice parameter a=4·10 Å. A few years later, the lattice structure was reported to be of the Cu_3Au type.[76] The atomic arrangement of the Al_3Sc phase is shown in Fig. 10. The structure can be described as ordered face-centred cubic (fcc), although in crystallographic terminology the Al_3Sc structure is actually a simple cubic lattice with four atoms (one Sc and three Al atoms) associated with each lattice point. This particular atomic arrangement is nominated $L1_2$ and is found in several intermetallic compounds, for instance Ni_3Al, Ni_3Fe and Cu_3Au.

Some efforts have been made in characterising the properties of the Al_3Sc phase. A compilation of some results is given in Table 3. The motivation for the majority of the investigations seems to be one of the three following:

(i) the Al_3Sc phase has a density of 3·03 g cm^{-3} and it melts peritectically at approx. 1320°C. This can make the Al_3Sc phase an attractive candidate as a material for lightweight high temperature structural applications[20,57,77–86]

(ii) in order to understand the effect of Al_3Sc precipitation in Al-alloys, it is necessary to gain more knowledge about the Al_3Sc phase[57,81,87–91]

(iii) the Al_3Sc is an excellent model phase for studying basic properties of intermetallic compounds.[79,90–98]

Table 3 Some reported properties of Al_3Sc phase

Reference	*E*, GPa (Young's modulus)	ν (Poisson's ratio)	CTE (Coefficient of thermal expansion), 10^{-6} K^{-1}	(111) APB energy, mJ m^{-2}	(100) APB energy, mJ m^{-2}
88	Approx. 111*				
20	166†	0·20†		Max. 670†	450†
79	166‡	0·22‡		313	
99	162·8†	0·204†			
	164·2±1·9‡	0·201±0·001‡			
89			16		

*Reported to decrease linearly with increasing temperature, to approx. 97 GPa at 550°C.
†Calculated.
‡Experimental.

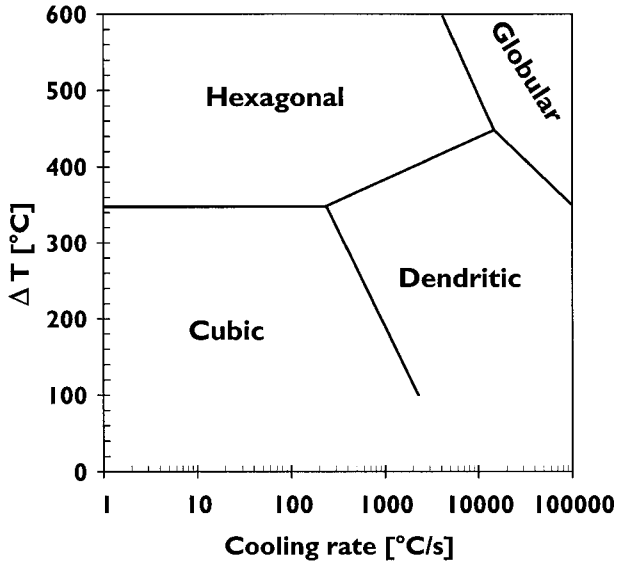

11 Morphology of primary Al_3Sc particles in Al–2 wt-%Sc alloy as a function of melt overheating and cooling rate during solidification: redrawn from Ref. 102

Formation of Al_3Sc in Al–Sc alloys

There are at least four ways that the Al_3Sc phase can form in dilute binary Al–Sc alloys.

1. Upon solidification of hypereutectic alloys (Sc > approx. 0·6 wt-%), Al_3Sc is the first phase to form.
2. The solidification of hypo- and hypereutectic alloys ends with formation of eutectic $Al + Al_3Sc$.
3. Al_3Sc can precipitate discontinuously from supersaturated solid solution.
4. Al_3Sc can precipitate continuously (nucleation and growth) from supersaturated solid solution.

Primary Al_3Sc

According to the binary phase diagram, primary Al_3Sc should form during solidification of all alloys with Sc content higher than approx. 0·6 wt-%, i.e. higher than the eutectic composition. Formation of primary Al_3Sc in Al–0·7 wt-%Sc melts cooled at 10^2–10^3 K s^{-1} has been reported.[18,32] According to the metastable state diagram,[32] this alloy composition is close to the eutectic one at these cooling rates.

Primary Al_3Sc is reported to have a highly faceted morphology.[13,18,100–102] The observation of a cubic morphology in a slowly cooled Al–8·7 wt-%Sc alloy indicates that the facet planes in this case are the crystallographic (100) planes.[13] Brodova *et al.*[100–102] have investigated the microstructure of rapidly cooled Al–2 wt-%Sc alloy. They found that the dominant morphology of primary Al_3Sc was dependent on both the cooling rate and the initial melt temperature. A map of primary Al_3Sc morphologies as a function of these parameters was constructed, and is redrawn in Fig. 11.

The nucleation mechanism and growth morphology of primary Al_3Sc in an Al–0·7 wt-%Sc alloy solidified at a cooling rate of 100 K s^{-1} were investigated by Hyde *et al.*[103,104] Indications were found that the primary Al_3Sc particles nucleate heterogeneously on oxide particles in the melt. The primary Al_3Sc particles were found to grow with a dendritic morphology, with the primary dendrite arms in the crystallographic ⟨110⟩ direction. The overall shape is cubic, which is in accordance with earlier observations.

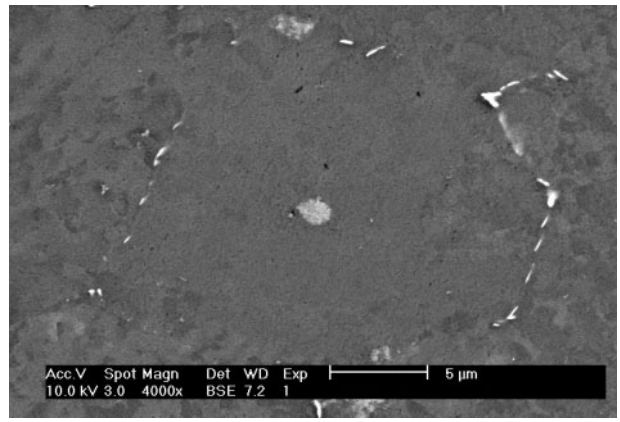

12 SEM image of particle structure of Al–0·7 wt-%Sc alloy cooled at a rate of 100 K s^{-1} during solidification as described in Refs 103 and 104; primary Al_3Sc particle is seen in centre of grain, whereas eutectic Al_3Sc is decorating grain boundaries; image is kindly provided by Dr Kristian Hyde, UMIST, Manchester, UK

Eutectic Al_3Sc

Eutectic $Al + Al_3Sc$ has been reported in hyper- as well as hypoeutectic alloys,[11] but is scantily described in the literature. Given a eutectic composition of 0·6 wt-%, a maximum solid solubility of Sc in Al of 0·35 wt-% and the specific densities in Table 1, a eutectic formed under equilibrium conditions would contain a volume fraction of approx. 0·63 vol.-%Al_3Sc. At high cooling rates, the volume fraction of Al_3Sc in the eutectic is probably somewhat smaller, owing to the increased supersaturation of Sc in Al.

The morphology of the eutectic in an Al–2 wt-%Sc alloy is reported to depend on the temperature of the melt before solidification.[100] For low melt temperatures, the eutectic is reported to be rodlike for a wide range of cooling rates. For intermediate melt temperatures and high cooling rates, a 'discontinuous eutectic' is reported, whereas for high melt temperatures and slow cooling rates, a 'quasieutectic' structure is reported, with Al_3Sc particles of almost spherical shape.

Hyde *et al.* have reported that during solidification of an Al–0·7 wt-%Sc alloy, some of the primary Al_3Sc particles are pushed ahead of the Al solidification front and end up at the grain boundaries.[103,104] Thus, primary Al_3Sc may be mixed with eutectic Al_3Sc in the microstructure. A scanning electron microscopy (SEM) picture showing eutectic Al_3Sc at the grain boundaries as described in Refs 103 and 104 is given in Fig. 12.

Discontinuous precipitation of Al_3Sc

Discontinuous precipitation of Al_3Sc from supersaturated solid solution is often observed in binary Al–Sc alloys.[13,18,31,105] This precipitation mechanism, which is sometimes referred to as cellular precipitation, is commonly described as a decomposition of supersaturated solid solution into α-Al and Al_3Sc at a moving grain boundary. The driving force for the grain boundary migration is the volume free energy that is released during the precipitation. As the grain boundary moves, it leaves behind a characteristic fan shaped array

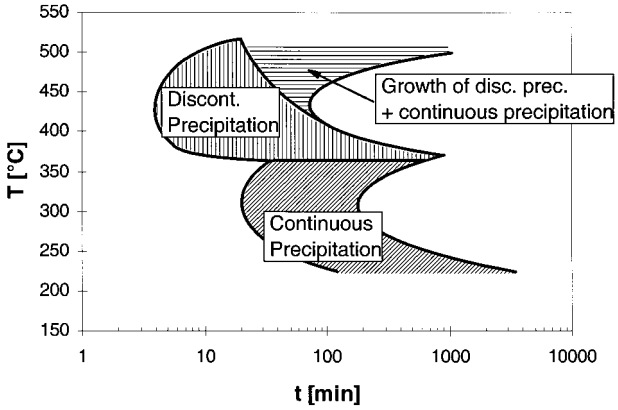

13 TTT diagram of precipitation in Al–0·2 wt-%Sc alloy after solutionising at 600°C and direct quench to aging temperature[31]

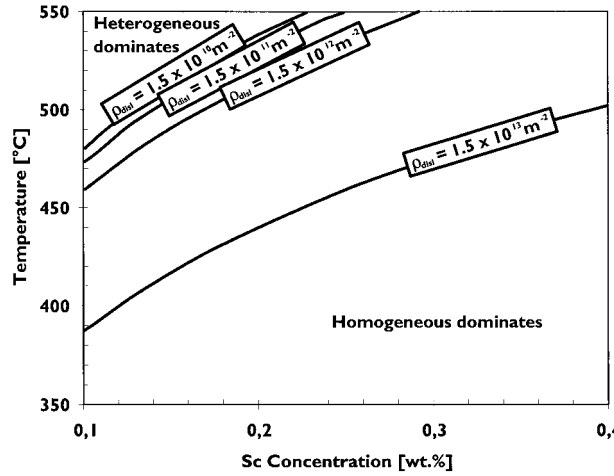

14 Nucleation map for binary Al–Sc alloys, which indicates how the tendency towards heterogeneous versus homogeneous nucleation is predicted to depend upon Sc concentration, transformation temperature and dislocation density: redrawn from Ref. 111

of precipitates. In the Al–Sc case, the discontinuously precipitated Al_3Sc particles have been demonstrated to be coherent with the aluminium matrix.[13,18]

The driving force for discontinuous precipitation increases with increasing supersaturation of Sc in the Al matrix. Thus, discontinuous precipitation in binary Al–Sc is most frequently reported in studies of alloys with a Sc content of 0·4 wt-% or higher.[13,18,106] Still, discontinuous precipitation has also occasionally been reported to occur at lower alloy compositions. In an Al–0·27 wt-%Sc alloy, discontinuous precipitation was observed over a wide range of temperatures.[107] In a recent study[31,105] of precipitation kinetics and mechanisms in Al–0·2 wt-%Sc, discontinuous precipitation was found to take place when the specimens were quenched directly from a solutionising temperature, in this case 600°C, to aging temperatures in the range 370–490°C. Further, C-curves in a temperature-time-transformation (TTT) diagram were established (Fig. 13) which showed that the highest transformation rate of discontinuous precipitation lies at a higher temperature than the highest transformation rate of the continuous precipitation reaction, i.e. the two precipitation reactions are represented by two separate 'noses' on the C-curves.

It has been shown that discontinuous precipitation can be suppressed by continuous precipitation if the material is cold worked before the precipitation heat treatment.[13,108]

As a result of their rather coarse nature and inhomogeneous dispersion, discontinuously precipitated Al_3Sc contributes but little to the strength of the alloy, and also leads to a smaller amount of Sc in supersaturated solid solution being available for subsequent continuous precipitation. Thus discontinuous precipitation is in general regarded as an undesired precipitation mode.

Continuous precipitation of Al_3Sc

Continuous precipitation of Al_3Sc is a bulk decomposition process of supersaturated solid solution of Sc in Al and can in the isothermal case be characterised by a nucleation stage, a growth stage, and finally a coarsening stage. Apparently, the continuous precipitation reaction occurs largely by homogeneous nucleation and diffusion controlled growth, and Al–Sc has occasionally been used as a model system for studying the mechanisms of nucleation, growth and coarsening.[107,109–111]

There have been several studies of the continuous precipitation reaction in binary Al–Sc alloys, and up till now there is no evidence that any metastable phases are forming before the $L1_2$ phase Al_3Sc. Thus it is assumed that the equilibrium phase nucleates directly from supersaturated solid solution.

Even though the nucleation of Al_3Sc is frequently reported to occur homogeneously throughout the Al matrix, there are some examples in the technical literature of reported heterogeneous Al_3Sc nucleation on dislocations[110,112–115] and grain boundaries.[110,113,115–118] In a recent numerical modelling study of continuous precipitation in Al–Sc alloys,[111] the effect of heterogeneous nucleation on dislocations is accounted for. The model predicts that homogeneous nucleation dominates at high Sc concentrations and low transformation temperatures, whereas heterogeneous nucleation is predicted to dominate at low Sc concentrations and high transformation temperatures. Figure 14 shows a sketch of a nucleation map for Al–Sc. The shift between homogeneous and heterogeneous dominance in nucleation is dependent on the dislocation density, as indicated in the figure.

The shape of continuously precipitated Al_3Sc particles is most frequently reported to be spherical.[29,112,113,119–129] However, it seems that under certain conditions, the shape can differ from the spherical one. Drits *et al.*[130] reported both spherical and star shaped morphology. The star shaped precipitates had arms growing in the crystallographic ⟨110⟩-directions. (Star shaped Al_3Sc precipitates have also been found after some thermomechanical treatments of an Al–Mg–Sc–Zr alloy.[131]) In Ref. 128, precipitates of both cuboidal and spherical morphology are found to coexist after certain heat treatments. Cauliflower shaped precipitates as well as precipitates of spherical and cuboidal shapes are reported by Novotny and Ardell.[110] Bastow and Celotto[132] found large oblong Al_3Sc particles in an Al–0·1 wt-%Sc alloy after aging at 400°C for 24 h. A faceted shape is suggested in a high-resolution image of an $Al_3(Sc, Zr)$ precipitate in an Al–Mg–Mn–Zr–Sc alloy.[133] In a systematic high-resolution transmission electron

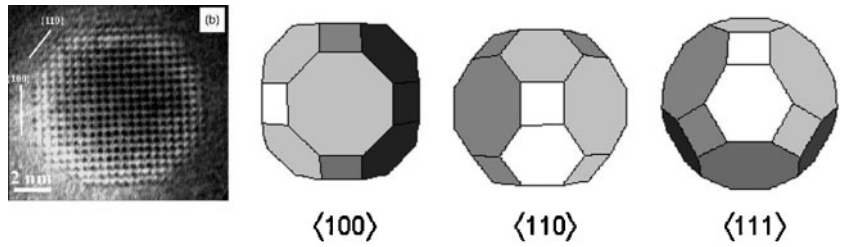

15 High resolution TEM picture along ⟨100⟩ axis of Al_3Sc particle in Al–0·3 wt-%Sc alloy aged at 300°C for 350 h[114] (reproduced with permission from Elsevier Science, image kindly provided by Dr E. A. Marquis and Professor D. N. Seidman), and various projections of a Great Rhombicuboctahedron

microscopy (TEM) study of the Al_3Sc particle morphology development during precipitation heat treatment of binary Al–Sc alloys by Marquis and Seidman,[114] it is demonstrated that the precipitates can take a wide range of shapes as they grow depending on Sc content in the alloy, transformation temperature and transformation time. Irregular shaped, star shaped and cuboidal shaped precipitates were observed under some conditions. It was, however, found that the equilibrium shape of the particles is an equiaxed multifaceted one (Fig. 15). Supported by Wulff's construction, it was concluded that the shape was that of a Great Rhombicuboctahedron. This equilibrium morphology has been reproduced by computer-simulations of particle growth.[87,134] The multifaceted particles can easily be taken for spherical in a conventional TEM picture.

Kinetics of precipitation of Al_3Sc from supersaturated solid solution

The precipitation kinetics of Al_3Sc in binary Al–Sc alloys is dependent on the precipitation heat treatment temperature and on the Sc content in the alloy. A comprehensive overview over the transformation kinetics in terms of C-curves is given by Zakharov.[135] The C-curves for 5% transformation for a range of Al–Sc alloys are redrawn in Fig. 16.

Hyland[107] studied the homogeneous nucleation kinetics of Al_3Sc in a Al–0·18 wt-%Sc alloy after direct quench from 650°C to precipitation temperatures of 288 and 343°C. He found that after an incubation time τ, the Al_3Sc particles nucleated at a constant rate until the diffusion fields of the individual particles started to overlap. At 288°C, the incubation time and time to significant diffusion field overlap were estimated to be approx. 24·5 and 150 min, respectively, whereas the corresponding values at 343°C were estimated to be approx. 7 and 20 min, respectively.

If one assumes that the Johnson–Mehl–Avrami–Komolgorov (JMAK) relationship is valid for this precipitation reaction, one can express the fraction transformed X as a function of the reaction time t by the equation

$$X(t) = 1 - \exp[-k(Dt)^n] \quad (1)$$

where k is a constant, D is the interdiffusion constant of Sc in Al, and the exponent n is dependent on the nucleation rate. For the situation described by Hyland[107] where the precipitates nucleate at a constant rate, the value of n should theoretically[136] be equal to 5/2.

Røyset and Ryum[31,105] applied an alloy and heat treatment method practically equal to that of Hyland.[107] One should thus expect that the precipitation kinetics should also be quite similar. However, Røyset and Ryum reported that the exponent n of the JMAK relationship was approx. 1·65–1·85 for the temperature range of concern.[31,105] This does not point in the direction of a constant nucleation rate, but rather in the direction of site saturation, i.e. that all the particles are nucleated simultaneously, which in the JMAK equation would yield an exponent n of 3/2.[136] An overview of some reported values of n in the JMAK equation is given in Table 4. The majority of the values lie closer to 3/2 than to 5/2. However, it is important to

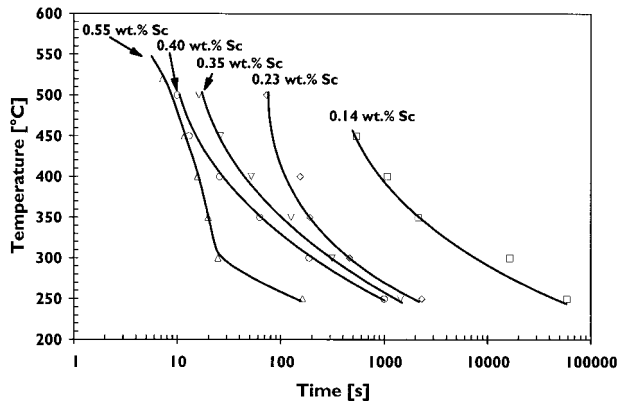

16 C-curves for 5% transformation in a range of binary Al–Sc alloys; redrawn from Ref. 135

Table 4 Some reported values of *n* in JMAK equation

Reference	*n*	C^0_{Sc}, wt-%Sc	T_{trans}, °C	Note
137	1·3	0·30	300	Solution heat treated (SHT) 500°C
	1·6/0·26	0·30	300	SHT 600°C. Low *n* at late stage
	2·0/0·26	0·30	300	SHT 640°C. Low *n* at late stage
29	1·30–1·49	0·15	260–370	
	1·45–1·96	0·25	260–370	
138	1·88–2·16	0·20	240–350	
31	1·65–1·85	0·23	270–350	SHT 600°C. Direct quench to transformation temp.

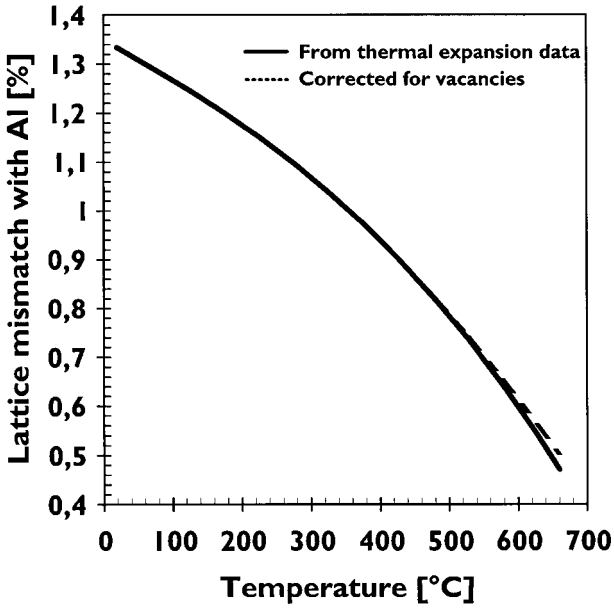

17 Lattice mismatch between Al and Al_3Sc as a function of temperature: solid line represents calculation based on linear thermal expansion of the two phases; dotted line represents correction for vacancies in Al lattice

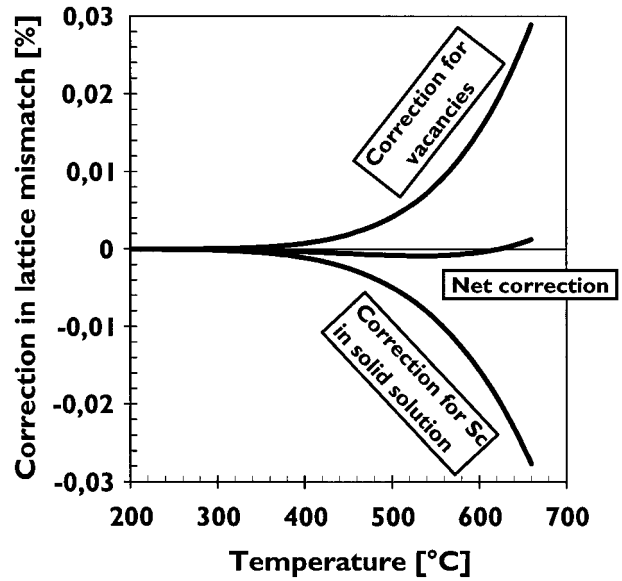

18 Corrections of mismatch calculated from linear thermal expansion data as a result of vacancies and to Al lattice expansion from Sc in solid solution

note that an n value close to 3/2 is *per se* not evidence of site saturation.

Hyland also showed that a water quench from the solutionising temperature significantly altered the nucleation kinetics in the subsequent precipitation heat treatment.[107] The incubation time was dramatically shortened, which is attributed to the quenched-in excess vacancies, and it is also indicated that there might be a shift in the nucleation rate in the early stage of precipitation. It is suggested that the vacancies may enhance the diffusion of Sc in Al, and that there is a possibility that vacancy clusters act as heterogeneous nucleation sites for Al_3Sc precipitates.[107] Regardless of which mechanism that is operative, it is clearly demonstrated that the nucleation kinetics can be dependent on the thermal history between solutionising and precipitation heat treatment.

Loss of coherency during growth of Al_3Sc precipitates

When an Al_3Sc particle grows, it will sooner or later reach a critical size where it will be energetically more favourable to introduce an interface dislocation at the Al/Al_3Sc interface than to increase the matrix strain. A simple approximation for the critical size can be derived from the lattice parameters, assuming that the critical size is reached when the misfit over the whole particle diameter equals the Burgers vector of the Al matrix

$$d_{\text{crit}} = \boldsymbol{b}/\delta \tag{2}$$

where $\boldsymbol{b}$ is the Burgers vector of Al and δ is the misfit between Al and Al_3Sc. This approximation yields a critical diameter of approx. 21·5 nm at ambient temperature.

The misfit δ and thus also the critical diameter d_{crit} will depend on the temperature, owing to the differences in thermal expansion between the Al matrix and the Al_3Sc particles. The thermal expansion of Al_3Sc has recently been measured,[89] and based on the differences in thermal expansion between Al[139] and Al_3Sc, the misfit as a function of temperature has been calculated.[89] This calculation is reproduced and shown by the solid line in Fig. 17.

It is, however, possible to refine this calculation somewhat.[140] Whereas the thermal expansion of Al_3Sc is expected to be only because of lattice expansion, there is a significant contribution from vacancies on thermal expansion of Al at high temperatures.[141] Thus, the temperature effects on the misfit should be calculated from the changes in lattice parameters rather than from the linear thermal expansion. By subtracting the vacancy effect on the thermal expansion one achieves a temperature-dependent misfit as represented by the dotted line in Fig. 17.

A second correction that should be taken into account is the effect of Sc in solid solution on the lattice parameter of the Al matrix. With increasing temperature, more Sc is brought into solid solution, and it is reported that the lattice parameter of the Al matrix, presumably measured at room temperature, increases linearly with the Sc content in solid solution.[142] These data can be used to calculate the effect on the lattice parameter at elevated temperatures under the assumption that the relative increase in lattice parameter owing to Sc in solid solution is independent of temperature. In Ref. 142, a figure is presented which shows the measured lattice parameter as a function of Sc content in solid solution, and a value $(da/dc)/a$ is reported, where a is the lattice parameter of the Al matrix and c is the Sc content in solid solution in at.-%. The reported value for $(da/dc)/a$ is 100 times larger than that indicated in the corresponding figure, possibly as a result of a decimal error in the text. Thus, in the present exercise, 1/100th of the reported value for $(da/dc)/a$ is used. Using this in combination with the regular solution approximation for the solvus line of Sc in Al,[12,31] one obtains a correction for Sc in solid solution on the temperature-dependent misfit as shown in Fig. 18. This figure shows

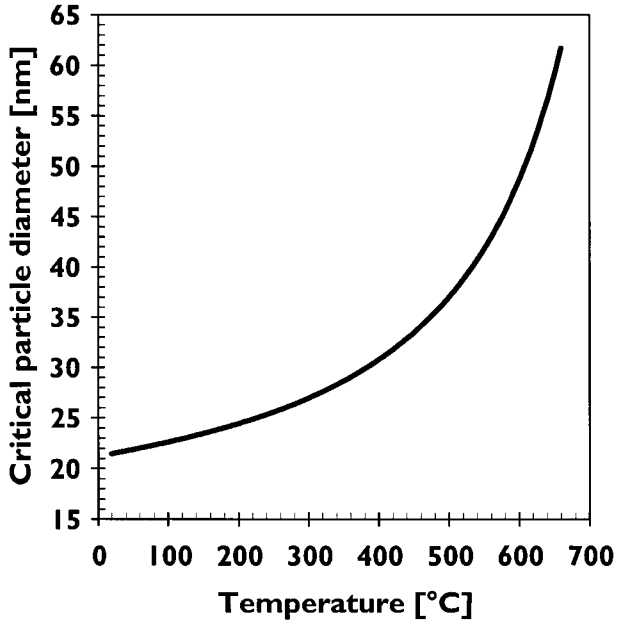

19 Simple approximation for temperature-dependent critical diameter for introduction of dislocations on Al/Al_3Sc interface

both the correction for vacancies and for Sc in solid solution on the same graph. The two corrections are of approximately the same magnitude, but with opposite signs. Thus, the resulting (net) correction is close to zero, and it turns out that the first hand approximation as applied in Ref. 89 is very good in this case.

Applying the calculated temperature dependent misfit with the simple approximation for a critical diameter for loss of coherency, one obtains a temperature-dependent critical diameter as shown in Fig. 19.

Some examples from the literature of experimentally observed critical diameters in binary Al–Sc alloys are summarised in Table 5, along with some predictions for critical diameters from Fig. 19. There is a fairly good consistency between the observations, and the measured diameter is quite close to the simple predictions above.

A more refined analysis on the transition from coherent to incoherent particles has recently been performed.[145] This analysis is based on the balance between the increase in particle/matrix interface energy owing to interfacial dislocations and the relaxation in elastic energy in the Al matrix owing to the same dislocations. This method yields a predicted critical diameter of 24·6 nm for transition from coherent to semi-coherent particles at ambient temperature. The temperature dependence of the critical diameter is not treated in this analysis.

Table 5 Some reported critical diameters for coherency loss in binary Al–Sc and corresponding theoretical critical diameters from Fig. 19

Reference	d_{crit}, nm	C^0_{Sc}, wt-%Sc	T_{trans}, °C	Theoretical d_{crit}, nm
119	38–40	0·5		
137	28–30	0·3	400	30·8
128	>32	0·2	400, 450	30·8, 33·5
129	50	0·2		
143	40	0·12, 0·25		
115	40	0·25	450–500	33·5–37
114	40	0·3	400, 450	30·8, 33·5
144	40	0·2	400–460	30·8–34·1
145	30–80	0·2	400–490	30·8–36·2

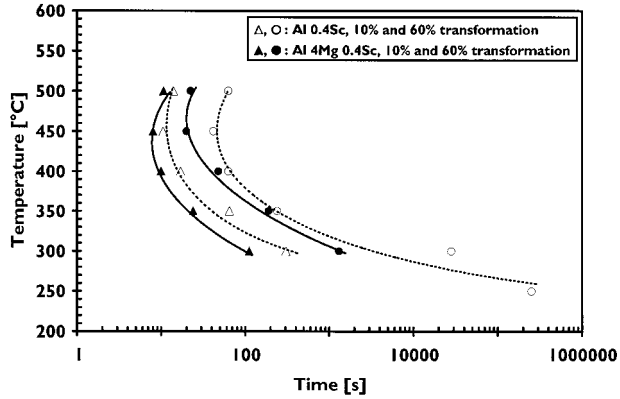

20 C-curves for 10% and 60% transformation in Al–0·4 wt-%Sc and Al–4 wt-%Mg–0·4 wt-%Sc: redrawn from Ref. 135

The loss of coherency during isothermal annealing has been reported to be accompanied by an increased average coarsening rate.[119,121,137,145] The increased coarsening rate has been attributed either to diffusion of Sc along dislocation lines[119,121] or to the increased particle/matrix interface energy of a semicoherent particle.[145] However, there are also several data sets in the literature that do not indicate an increased growth rate after the loss of coherency.[114,128]

Al_3Sc/Al interface energy

The interface energy between Al_3Sc and the Al matrix is one of the key parameters that governs the nucleation, growth and coarsening behaviour of Al_3Sc in Al and Al alloys. The interface energy has been estimated in several investigations, either by fitting experimental data to equations that describe nucleation or coarsening, or by calculations. A compilation of some of the results is given in Table 6. There is considerable spread in the reported values, regardless of what approach has been used for the estimation.

Influence of other elements on precipitation of Al_3Sc

Magnesium

With regard to precipitation mechanism, it has been stated that Mg suppresses the tendency to discontinuous precipitation of Al_3Sc.[106] In an investigation of precipitation kinetics of Al_3Sc in the temperature range 300–500°C, only minor changes in the kinetics (Fig. 20) were found when up to 5 wt-%Mg was added to an Al–0·4 wt-%Sc alloy.[135] It seems that the precipitation reaction is slightly faster in the Mg-containing alloys.

Several investigations on age hardening response also imply that there is only a small, if any, effect of Mg on the precipitation kinetics of Al_3Sc.[23,148,149] It is, however, found that the hardness increase from the precipitation of Al_3Sc is somewhat reduced in Al–Mg–Sc alloys compared to binary Al–Sc alloys.[23,148,149] In Ref. 149, it is suggested that some of the Sc is dissolved in the Al_3Mg_2 phase, and thus the age hardening potential is reduced with increasing Mg content. Somewhat contradictory to these observations, but

sustained by Ref. 135, it has recently been reported[150] that precipitation of Al_3Sc at 300 and 350°C occurs slightly faster in an Al–2 wt-%Mg–0·2 wt-%Sc alloy than in an Al–0·2 wt-%Sc alloy studied previously by the same researchers,[117,118] and that the corresponding hardness increase is highest in the Al–Mg–Sc alloy. The only reported difference in experimental procedure is the solutionising temperature, which was higher for the Al–Sc alloy (648°C) than for the Al–Mg–Sc alloy (617°C). However, given that the nucleation time is shortened by quenched-in vacancies as suggested by Hyland,[107] the difference in homogenisation temperature should be in favour of a faster precipitation of the binary Al–Sc alloy. It should be worthwhile to probe deeper into this observation of different aging responses.

Mg in solid solution increases the lattice parameter of the Al matrix. This is in turn expected to influence the critical diameter for Al/Al_3Sc coherency loss, as discussed in the section on 'Loss of coherency during growth of Al_3Sc precipitates' above. Such an influence on the critical diameter is also briefly discussed elsewhere.[150] A critical diameter of 80 nm in an Al–3 wt-%Mg–0·2 wt-%Sc alloy has been observed, compared to 40 nm in a binary Al–0·2 wt-%Sc alloy of the same investigation.[144] Other researchers have reported a critical diameter in excess of 116 nm in an Al–6·3 wt-%Mg–0·2 wt-%Sc alloy.[151]

Computer simulations predict that the Al/Al_3Sc interface should be enriched in Mg.[87] These predictions are confirmed experimentally by three-dimensional atom probe microscopy of an Al–2 wt-%Mg–0·2 wt-%Sc alloy aged at 300°C.[38] Here, it was found that the Mg content at the interface is approximately three times higher than the matrix concentration, regardless of aging time.

Copper

It has been claimed that Cu suppresses the tendency towards discontinuous precipitation of Al_3Sc.[106] Zakharov and Rostova[152] have reported that additions of up to 1·4 wt-%Cu have only minor effects on the precipitation kinetics in an Al–0·4 wt-%Sc alloy. The most noticeable effect is that for temperatures above 400°C, the late stage of the transformation is slowed down for the highest Cu contents. This does not show in Fig. 21, however, where only the 10% and 60% transformation curves are included.

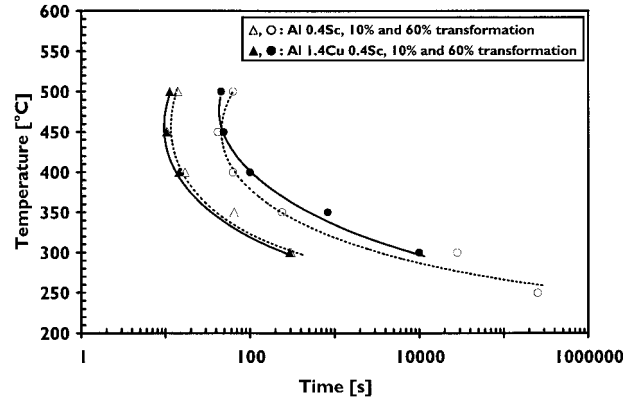

21 C-curves for 10% and 60% transformation in Al–0·4 wt-%Sc and Al–1·4 wt-%Cu–0·4 wt-%Sc: redrawn from Ref. 152

The W-phase (Al,Cu,Sc) was observed in the alloy with the highest Cu content, which means that less Sc is available for the precipitation of Al_3Sc in this alloy. Another investigation on the age hardening response of Al–0·23 wt-%Sc and Al–2·5 wt-%Cu–0·23 wt-%Sc at 300°C also implies that the precipitation behaviour of Al_3Sc in the two alloys is similar.[153,154] At 350°C, a limited portion of the Al_3Sc has been observed to nucleate heterogeneously on coarse θ' precipitates.[155] According to the isothermal sections of the phase diagram[43] one should expect the ternary W-phase to form instead of the Al_3Sc phase in an alloy with such a high Cu/Sc ratio. However, no observations of the W-phase or other ternary phases were reported from TEM studies of the Al–2·5 wt-%Cu–0·23 wt-%Sc alloy that had been heat treated in the temperature range 300–460°C.[153–156] A third investigation on the precipitation in Al–0·48 wt-%Sc alloys with up to 4·40 wt-%Cu in the temperature range 100–450°C also concludes that no W-phase or other ternary phase forms during the heat treatment.[157]

Copper in solid solution decreases the lattice parameter of the Al matrix. Thus, it is expected that the misfit between Al and Al_3Sc precipitates should be higher in

Table 6 Reported values of interphase energy $\gamma_{Al/Al3Sc}$ between coherent Al_3Sc precipitates and Al matrix

Reference	$\gamma_{Al/Al3Sc}$, mJ m^{-2}	Method of estimation
137	10	Fit of coarsening data to Lifshitz–Slezev equation
107	78±20 (288°C) 93±20 (343°C)	Back-calculation of incubation time
107	123±41 (288°C) 125±35 (343°C)	Back-calculation of nucleation rate
29	54·2 (400°C) 63·2 (430°C) 41·3 (460°C)	Fit of coarsening data to Ostwald ripening
146	$\gamma_{(100)}$: 192 (0 K) $\gamma_{(111)}$: 226 (0 K)	Pseudopotential calculations
147	$\gamma_{(100)}$: 32·5 (0 K) $\gamma_{(110)}$: 51·3 (0 K) $\gamma_{(111)}$: 78·2 (0 K) $\gamma_{(100)}$: 31·5 (288°C) $\gamma_{(100)}$: 32·5 (343°C)	Atomistic simulation
110	105	Fit of coarsening data to LSW theory
31	20–300	Fit of coarsening data to Ostwald ripening for 16 different temperatures
111	57	Fit of precipitation model to experimental data*
145	120, coherent particles 170, semicoherent particles	Fit of coarsening data

*It is argued in this study that γ may be lower in the nucleation stage.

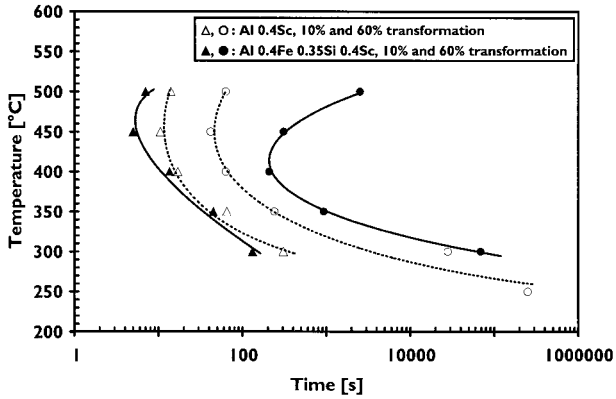

22 C-curves for 10% and 60% transformation in Al–0·4 wt-%Sc and Al–0·4 wt-%Fe–0·35 wt-%Si–0·4 wt-%Sc: redrawn from Ref. 135

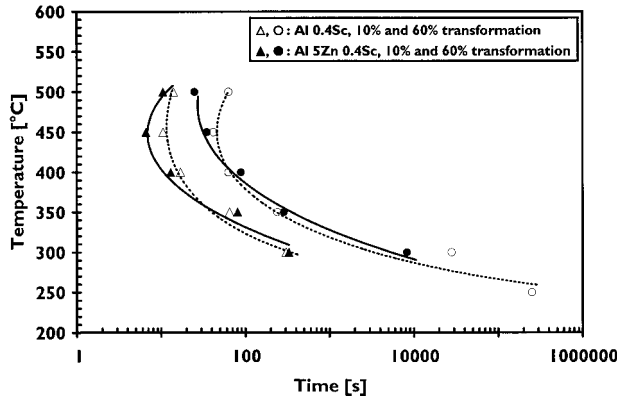

23 C-curves for 10% and 60% transformation in Al–0·4 wt-%Sc and Al–5 wt-%Zn–0·4 wt-%Sc: redrawn from Ref. 135

Al–Cu–Sc alloys compared to Al–Sc alloys. However, an experimental investigation of Al–2·5 wt-%Cu–0·23 wt-%Sc alloy comes to a different conclusion. The lattice misfit strain is found to decrease compared to Al–0·2 wt-%Sc, and the critical diameter for coherency loss was found to be the same in the ternary and the binary alloy.[144] It is suggested that these observations may be because of the dissolution of some Cu in the Al_3Sc phase, and thus that the lattice parameters of both the Al matrix and the Al_3Sc precipitates decrease in the ternary alloy.

Silicon

It has been found that the onset of precipitation in Al–0·4 wt-%Sc is only slightly altered when Si contents of up to 0·4 wt. are introduced in the alloy. However, the final stage of the precipitation reaction is considerably delayed with increasing Si content.[135] Figure 22 shows the effect of addition of a joint of 0·35 wt-%Si and 0·40 wt-%Fe. There are at least two possible explanations for why an Si-addition leads to this behaviour.

1. Alloying with Si is known to promote discontinuous precipitation of Al_3Sc.[106,158] It has been shown that when isothermal precipitation of Al_3Sc starts discontinuously, the later stage of the overall transformation can be very slow.[31]

2. The isothermal section of the phase diagram suggests that the V-phase ($AlSc_2Si_2$) should form in alloys of this composition.[46] If the V-phase forms, less Sc is available for precipitation of Al_3Sc.

It has been shown[157] that for an Al–Sc–Si alloy with solid solution content of 0·10 wt-%Sc an 1·10 wt-%Si, the only phases to precipitate after heat treatment at 200°C are Si and an (Al,Sc,Si)-phase, possibly the V-phase. On the other hand, the Al_3Sc phase has been observed to form in alloys with 0·4 wt-%Sc and up to 0·8 wt-%Si.[159,160]

Zinc

It has been reported that additions of up to 5 wt-% Zn have only minor effects on the precipitation kinetics of an Al–0·4 wt-%Sc alloy[135] (Fig. 23). In Ref. 106, it is claimed that Zn promotes discontinuous precipitation of Al_3Sc.

Lithium

A comparison of the age hardening response at 400°C in Al–2·4 wt-%Li–0·19 wt-%Sc and Al–0·24 wt-%Sc alloys indicates that the onset of Al_3Sc-precipitation is not affected by the presence of Li.[161]

Zirconium

As mentioned in the section on 'Ternary phase diagrams with dispersoid-forming elements' earlier, a considerable amount of Zr is dissolved in the Al_3Sc phase and thus a more correct denotation of the precipitating phase is $Al_3(Sc_{1-x}Zr_x)$. In discussing the influence of the Zr content on the precipitation of Al_3Sc, one is therefore actually discussing the difference in precipitation of Al_3Sc versus $Al_3(Sc_{1-x}Zr_x)$.

It is found that an addition of 0·15 wt-%Zr to an Al–0·4 wt-%Sc alloy only marginally affects the initial stage of the precipitation reaction,[123,135] while it slows down the later stages of the transformation considerably (Fig. 24).[135] The coarsening rate of the $Al_3(Sc_{1-x}Zr_x)$ particles in Al–Sc–Zr alloys is found to be much slower than that of Al_3Sc particles in Al–Sc alloys.[123,162]

In three-dimensional atom probe field ion microscopy (3D-APFIM) of $Al_3(Sc_{1-x}Zr_x)$ particles formed at 475°C in a ternary Al–Sc–Zr alloy,[163] it was found that the core of the particles is almost pure Al_3Sc whereas there is a shell of $Al_3(Sc_{1-x}Zr_x)$ with almost equal content of Sc and Zr. Such a behaviour has also been predicted by computer modelling of precipitation of $Al_3(Sc_{1-x}Zr_x)$ at 480°C in an Al–Zn–Mg–Sc–Zr alloy.[164] This model predicts that Zr starts to enter the growing

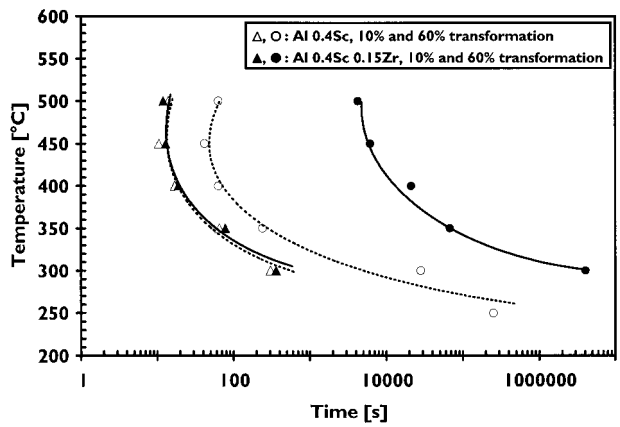

24 C-curves for 10% and 60% transformation in Al–0·4 wt-%Sc and Al–0·4 wt-%Sc–0·15 wt-%Zr; redrawn from Ref. 135

$Al_3(Sc_{1-x}Zr_x)$ particles when approximately half of the supersaturated Sc has been precipitated. The Zr content of the outer shell is predicted to be much higher than what has been found experimentally.[163,164]

Another 3D-APFIM study of $Al_3(Sc_{1-x}Zr_x)$ particles in a ternary Al–Sc–Zr alloy has been reported.[165] Here, particles grown at 300°C for various lengths of time were studied. The Zr content in these particles was much lower than that reported/predicted at higher temperatures,[163,164] even after very long annealing times.

Iron

The effect of adding up to 0·7 wt-%Fe on the precipitation kinetics in an Al–0·4 wt-%Sc alloy has been investigated.[135] The onset of precipitation was only slightly influenced by the Fe-level whereas the later stages of the transformation, however, were significantly slowed down as the Fe-level increased. An example of the effect of a joint addition of Fe and Si is shown in Fig. 22.

Manganese, chromium and titanium

Small additions (<0·3 wt-%) of manganese or chromium to Al–0·40 wt-%Sc alloys are reported to have only minor effects on the precipitation kinetics of Al_3Sc.[135] According to Ref. 106, Mn is reported to promote, and Cr and Ti to suppress discontinuous precipitation.

Rare earth elements

An investigation of the precipitation behaviour of Al–0·3 at.-%Sc and Al–0·3 at.-%Sc–0·3 at.-%X alloys, where X is either yttrium, gadolinium, holmium or erbium, in the temperature range 235–310°C indicated that a $Al_3(Sc_{1-x}X_x)$ phase with $L1_2$ structure was formed in the ternary alloys.[22] Peak strength is reported to occur after approx. 10 h at 285°C in all alloys, which indicates that the precipitation kinetics up to peak strength is practically unaltered by the ternary additions.

Influence of Sc on microstructure and properties of wrought aluminium alloys

Most of the effects of Sc addition in wrought Al-alloys are linked to the formation of the Al_3Sc phase. In a typical processing route of a wrought aluminium alloy, particles of the Al_3Sc phase can form under three different conditions, each of which influences the microstructure and properties of the alloy in a specific way:

1. During solidification after casting or welding, Al_3Sc particles can form in the melt and act as nuclei for α-Al, thus leading to grain refinement.[18,166]

2. High temperature processing of the alloy in the range 400–600°C, for instance homogenisation, hot-rolling or extrusion, can give a dense distribution of Al_3Sc particles of typically 20–100 nm size. The particle distributions formed under such conditions are reported to lead to good recrystallisation resistance[128,148,167,168] and enhanced superplasticity.[52,169,170]

3. Heat treatment in the range 250–350°C can lead to significant precipitation hardening of an alloy supersaturated in Sc.[148,158,171] The size of strengthening Al_3Sc precipitates is typically in the range 2–6 nm.[121]

Grain refinement

A good grain refinement is almost always desired upon solidification. The formation of small, equiaxed grains rather than long dendrites in the melt facilitates the feeding of the melt into cavities of the shrinking solidified metal, and thus reduces the problem of shrinkage porosity. The tendency to hot cracking is also reduced, and the second phase particles become more finely and uniformly distributed.

To the authors' knowledge, the first effect of Sc in Al-alloys that was reported in an international scientific journal was the grain refining action in pure Al and in an Al–Cu alloy upon solidification,[172] which was found to be stronger for Sc than for other transition metals. In later studies of Sc as a grain refiner in pure Al,[18,32,173] it has been demonstrated that approx. 0·7 wt-%Sc is sufficient to provide excellent grain refinement. It has also been demonstrated that additions of 0·25 wt-%Sc + 0·25 wt-%Zr provide good grain refinement in pure Al.[18]

In order for Sc to act as an effective grain refiner, the Al_3Sc phase has to form in the melt before the solidification of α-Al. The Al_3Sc particles have a lattice parameter close to that of pure Al, and when hypereutectically formed, the Al_3Sc particles are very effective substrates for the nucleation of the α-Al phase. As mentioned in the section on 'Formation of Al_3Sc in Al–Sc alloys' above, this requires that the alloy is hypereutectic with respect to Sc, i.e. in excess of approx. 0·6 wt-% in a binary Al–Sc alloy. In ternary and higher order systems, the eutectic Sc composition may depend on the other alloying elements present. For instance, the eutectic composition of Sc has been predicted to decrease with increasing Mg content in the ternary Al–Mg–Sc system.[39] This prediction is sustained by the observation of good grain refinement by adding 0·5 wt-%Sc to an Al–7 wt-%Mg alloy.[174] (Other examples of grain refinement at Sc concentrations lower than that of the binary eutectic are found in Ref. 173.)

Similarly, the observation of good grain refinement in an Al–0·25 wt-%Sc–0·25 wt-%Zr alloy[18] may be as a result of a lower Sc content of the eutectic in the ternary system, i.e. less Sc is needed to make the alloy hypereutectic. No literature data on the liquidus surface of the Al–Sc–Zr system are available, and thus this hypothesis cannot be confirmed. In more complex alloy systems, it is also observed that excellent grain refinement is achieved at low Sc contents when Sc is added together with Zr. It is reported that adding either 0·2 wt-%Sc, 0·6 wt-%Sc or 0·1 wt-%Zr to an Al–5%Mg alloy gives much poorer grain refinement than adding 0·2 wt-%Sc + 0·1 wt-%Zr.[175] Similarly, additions of 0·15 wt-% of either Sc or Zr are reported to only marginally refine the grain structure in an Al–Cu–Li alloy, whereas a joint addition of 0·15 wt-%Sc and 0·15 wt-%Zr gives excellent grain refinement.[176] For an AA 365·0 casting alloy (Al–7 wt-%Si–0·4 wt-%Mg), good grain refinement is achieved by adding 0·39 wt-%Sc or 0·27 wt-%Sc + 0·19 wt-%Zr.[177] In some Al–Zn–Mg–Sc–Zr alloys, it is also found that an addition of 0·2–0·3 wt-%Sc can be sufficient for good grain refinement.[166,169,178,179] Examples of the grain refinement as a function of Sc addition in pure Al and in an Al–Zn–Mg–Zr alloy are shown in Fig. 25.

The nucleation of α-Al on Al_3Sc particles in the melt is facilitated by the close match in the lattice parameters of the two phases. As shown in Fig. 17, the mismatch at the

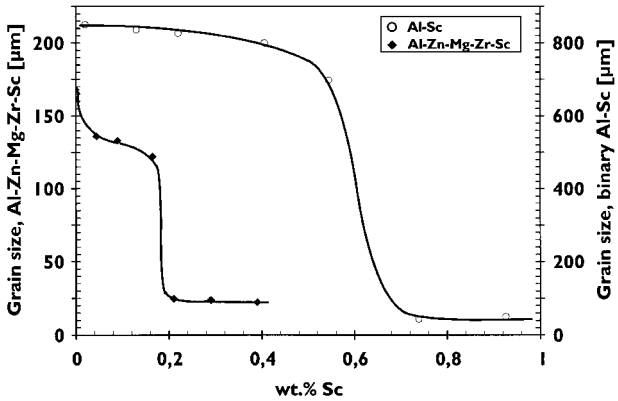

25 Grain refinement as a function of Sc addition in pure Al (redrawn from Ref. 32) and Al–Zn–Mg–Zr (redrawn from Ref. 169); note that data points are plotted on different ordinate axes

eutectic temperature of binary Al–Sc alloys (660°C) is only approx. 0·47%. In Refs. 57 and 89, it is shown that when Zr, Hf and in particular Ti is dissolved in the Al_3Sc particles, this reduces the lattice parameter of the phase. It appears that when 25% of the Sc atoms in Al_3Sc are substituted by Ti, the mismatch is zero at approx. 550°C and becomes negative at higher temperatures.[89] This suggests that by carefully selecting the Ti content of the alloy, it should be possible to obtain $Al_3(Sc,Ti)$ substrates in the melt that match exactly the lattice parameter of the nucleating α-Al, and thus further improve the grain refinement of the alloy. This appears to have been achieved in a recent work,[180] where the grain refinement of an Al–0·7 wt-%Sc alloy was compared with that of an Al–0·5 wt-%Sc–0·2 wt-%Ti alloy. At a cooling rate of 100 K s^{-1}, only an estimated 2% of the primary Al_3Sc particles of the binary Al–Sc alloy were effective nuclei compared to practically 100% for the primary $Al_3(Sc,Ti)$ particles in the ternary Al–Sc–Ti alloy, leading to a much smaller grain size in the ternary alloy. Whereas the match of lattice parameters may be of importance for these results, the authors of this investigation[180] draw attention to other factors such as different growth restriction factors for Sc and Ti, and the possibility of a peritectic reaction in the ternary alloy. Nevertheless, the principle of matching lattice parameters is worth looking into further in future work.

Effects from dispersoids

'Dispersoids' is a term which is commonly used about the classes of second phase particles that are formed in an Al alloy during high temperature annealing or thermomechanical processing such as homogenisation, hot rolling, extrusion and forging. A dense distribution of dispersoids can give a significant contribution to an alloy's strength owing to particle strengthening, but this is rarely the main strengthening mechanism. A more important contribution from the dispersoids is their ability to stabilise the grain/subgrain structure of an alloy through the Zener-drag action, and thus improve the mechanical properties of the alloy.

There are two noticeable dispersoid-related effects that have been reported for Sc-containing alloys. The first is the stabilising effect on a deformed microstructure. When a non-recrystallised structure is preserved in an alloy, this can add considerably to the mechanical strength of the material. The second effect is the preservation of a small grain size during hot deformation at slow deformation rates, which is necessary to obtain superplastic properties of an Al-alloy.

Recrystallisation resistance

The anti-recrystallisation effect of Sc was first published in a patent[171] where 0·3 wt-%Sc was added to pure Al and to Al–Mg, Al–Mn and Al–Zn–Mg alloys. Both Sc-free and Sc-containing materials were cold worked and subsequently annealed and it was found that the addition of Sc increased the temperature for onset of recrystallisation by approx. 220°C in pure Al and somewhat less in the Al-alloys. Although the author of the patent[171] may have been well aware that the anti-recrystallisation effect is caused by Al_3Sc dispersoids, this is not mentioned in the text. The first journal paper that explicitly points out that the recrystallisation resistance is due to Al_3Sc dispersoids was an investigation of the effects of adding Sc to wrought Al–Mg alloys.[181] In this work, it was found that the Al_3Sc dispersoids were very effective in preventing recrystallisation up to temperatures of approx. 400–450°C. At higher temperatures, the dispersoids coarsen considerably and the microstructure was partially recrystallised.

It is established that the Zener-drag p_Z that is imposed on an advancing grain boundary by randomly distributed dispersoids can be expressed in the form

$$p_Z = k f / r \tag{3}$$

where k is a factor that includes the interface energy between the dispersoids and the matrix, f is the volume fraction and r is the mean radius of the dispersoids. Thus the Zener drag will decrease rapidly in the case where the dispersoids are coarsening.

As mentioned in the section on 'Influence of other elements on precipitation of Al_3Sc' above, the $Al_3(Sc_{1-x}Zr_x)$ dispersoids in a ternary Al–Sc–Zr alloy coarsen at a much slower rate than the Al_3Sc dispersoids in a binary Al–Sc alloy. This effect was first reported in Ref. 123 (although also observed in Ref. 182), and according to Ref. 33, the same authors demonstrated soon after that the denser dispersoid distribution achieved in an Al–Sc–Zr alloy leads to superior recrystallisation resistance compared to a binary Al–Sc alloy. An example of the increased recrystallisation resistance by adding both Zr and Sc is shown in Fig. 26.

In isothermal sections of the ternary Al–Sc–Zr phase diagram, it is indicated that the solid solubility of Sc+Zr is somewhat higher than that of Sc alone.[54] It has also been demonstrated, both by electrical conductivity measurements (Fig. 27) and microstructural observations, that the supersaturation of Sc+Zr is greater than that of only Sc or Zr in as cast Al–1·5%(Sc+Zr) alloys.[183] This indicates that it should be possible to increase the volume fraction of dispersoids in Al–Sc–Zr compared to Al–Sc. It is suggested[162] that the increased volume fraction that can be achieved by adding both Sc and Zr can be advantageous in conventional wrought Al-alloys.

There are at least two different conditions under which Al_3Sc or $Al_3(Sc_{1-x}Zr_x)$ dispersoids can form to prevent recrystallisation:

1. Sc (or Sc and Zr) is in solid solution before the deformation. In the case of cold deformation and

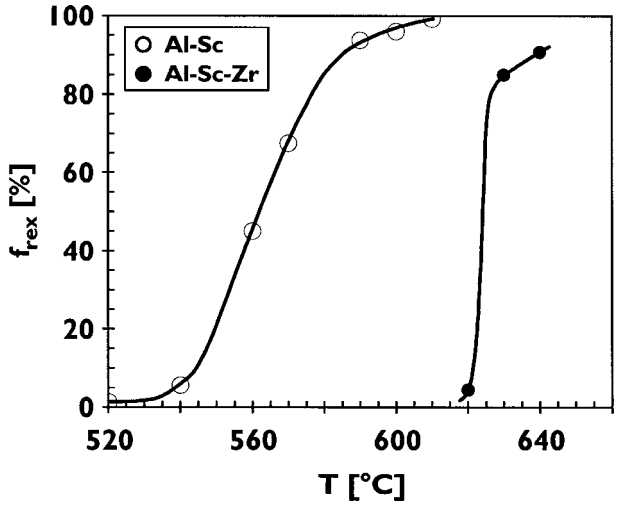

26 Fraction recrystallised structure in cold rolled sheets of Al–0·4 wt-%Sc and Al–0·4 wt-%Sc–0·15 wt-%Zr as a function of annealing temperature; redrawn from Ref. 183

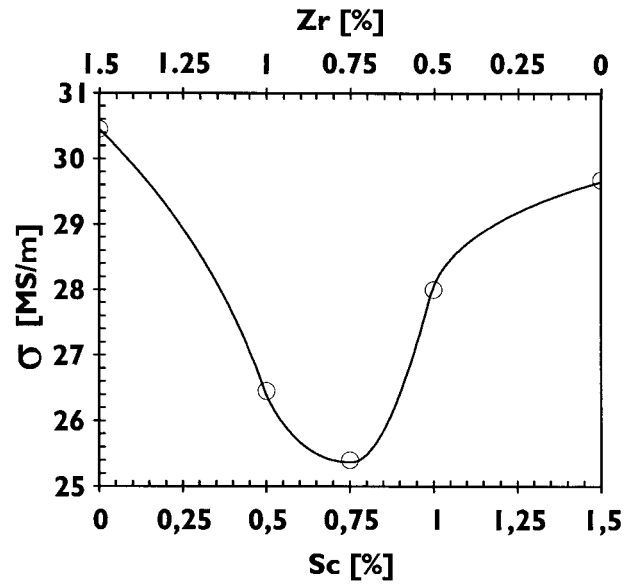

27 Electrical conductivity in Al–1·5%(Sc+Zr) alloys; redrawn from Ref. 183

subsequent annealing, the Al_3Sc or $Al_3(Sc_{1-x}Zr_x)$ dispersoids may nucleate and grow before the nucleation and growth of recrystallised grains takes place. Dispersoids can form after a direct up-quench to the annealing temperature,[115,143,148,184] during ramp-up to the annealing temperature[115] or by pre-annealing at an intermediate temperature.[129] In the case of hot deformation, the Al_3Sc or $Al_3(Sc_{1-x}Zr_x)$ dispersoids may nucleate and grow during preheating of the material and during the hot deformation itself.[184]

2. The Al_3Sc or $Al_3(Sc_{1-x}Zr_x)$ dispersoids are formed in the material before deformation.[184] Considering cold rolling and subsequent annealing, the annealing temperature T_{ann} may be either lower or higher than the temperature T_{disp} at which the dispersoids were formed. If $T_{ann}<T_{disp}$ only limited, if any, coarsening of the dispersoids is expected to take place and thus the Zener drag from the particles is expected to be practically constant. The driving force for recrystallisation, however, is expected to decrease somewhat with the annealing time as a result of recovery processes. Thus, if recrystallisation does not occur within short annealing times the material is expected to remain unrecrystallised for infinite time at the annealing temperature. If $T_{ann}>T_{disp}$ there will be substantial coarsening of the dispersoids during annealing. In order for the material to remain unrecrystallised, the decrease in driving force for recrystallisation owing to recovery has to be at least as rapid as the decrease in Zener drag because of particle coarsening.

Experimental comparisons of the conditions above point in the direction that the recrystallisation resistance is poorest when Sc (or Sc and Zr) is in solid solution before deformation and the deformed material is up-quenched to the annealing temperature[148] or when Al_3Sc or $Al_3(Sc_{1-x}Zr_x)$ dispersoids are formed before deformation at $T_{disp} \gg T_{ann}$.[184,185] Excellent recrystallisation resistance is achieved if dispersoids are formed at an intermediate anneal of solutionised and deformed material[128] or if dispersoids are formed at $T_{disp}<T_{ann}$ before deformation.[148,185–187] It seems that the decrease in Zener drag because of dispersoid coarsening in many cases is slower than the decrease in driving force for recrystallisation because of recovery processes. Thus there is an advantage in forming a high number density of small dispersoids, which for most practical cases means that they should be formed at $T_{disp} \ll T_{ann}$.[122]

When an advancing high angle grain boundary, i.e. the recrystallisation front, is passing a coherent Al_3Sc dispersoid, there are at least three possible grain boundary/dispersoid interactions.

1. The Al_3Sc dispersoid retains its global orientation relationship and thus loses its coherency with the surrounding matrix.
2. The Al_3Sc dispersoid rotates as the grain boundary passes, either by diffusional processes at the dispersoid/matrix interface or by the grain boundary passing through the dispersoid, and the Al_3Sc dispersoid assumes the same crystallographic orientation as the Al matrix of the recrystallised grain.
3. The Al_3Sc dispersoid dissolves at the grain boundary and re-precipitates in the recrystallised grain.

Which interactions that actually take place will probably depend on the dispersoid size, annealing temperature and driving force for recrystallisation. It is also possible that alloy composition (other elements than Al) is of importance.

It has been reported that large (Ø about 100–150 nm) Al_3Sc dispersoids in a deformed Al–4 wt-%Mg–0·2 wt-%Sc alloy annealed at 575°C lose the orientation relationship with the matrix after being passed by the recrystallisation front.[148]

A rotation of somewhat smaller Al_3Sc dispersoids in a recrystallising binary Al–0·25 wt-%Sc alloy has been reported.[115,143] The rotation was reported to be accompanied by substantial growth (from Ø 30 nm to Ø 48 nm) as a result of enhanced Sc diffusion at the grain boundary. Observations suggested that the grain boundaries were passing through the dispersoids, and thus the Al_3Sc dispersoids retained the orientation relationship with the recrystallised Al matrix.

Dissolution and re-precipitation of Al_3Sc dispersoids has been reported during recrystallisation of a 50% cold rolled Al–0·2 wt-%Sc alloy.[162] Large, spherical, partially

coherent dispersoids were observed to dissolve at the recrystallisation front and re-precipitate as smaller, coherent Al_3Sc cuboids.

Superplastic forming

It seems that the first publication on superplastic properties of Sc-containing Al-alloys was a study of an Al–3·5%Cu–1·4%Mg–0·45%Mn–0·4%(Sc + Zr) alloy.[188] It was recognised that the superplastic properties are a result of the stabilisation of the fine grain structure by Al_3Sc dispersoids. The Sc-containing Al alloys that have received most attention for their superplastic properties, however, are those of the Al–Mg–Sc system, which was first published in a patent.[189] Here, it was noted that an Al–4 wt-%Mg–0·5 wt-%Sc alloy had superior superplastic properties compared to fine-grained 7475 (Al–Zn–Mg–Cu alloy). Binary Al–0·5 wt-%Sc and Al–4 wt-%Mg alloys did not behave superplastically. The flow stress at the hot forming temperature was found to be much (30–40%) lower in the ternary alloy than that of the two binary alloys.

The superplastic properties of Al–Mg–Sc alloys have been explored by several research groups over the last decade.[190–196] It has frequently been found that the deformation mechanism is dominated by grain boundary sliding.[190] However, it has also been reported that Al–Mg–Sc alloy may deform superplastically without noticeable grain boundary sliding.[23] It is generally recognised that the grain boundary sliding mechanism is facilitated when the average grain size is very small and grain boundaries are predominantly high-angle. Such a microstructure may be achieved by careful thermomechanical processing of the starting material.[193,194,197,198] It has, however, been shown that a fine grained structure with high angle boundaries may develop during superplastic forming of Al–Mg–Sc alloys even if the starting microstructure is an entirely different one, for instance that of a cold rolled sheet.[192] It has also been suggested that superplastic forming of as cast material may be possible.[189]

One of the more efficient thermomechanical processes for achieving an ultrafine grain structure with high angle grain boundaries in Al-alloys is equal channel angular pressing (ECAP). A Japanese–American group of scientists has published an impressive body of research on improvements in superplastic properties in Al-alloys processed by ECAP over the last few years, and several of the publications are from investigations on Al–Mg–Sc alloys.[170,199–224] Maximum strains in excess of 2000% at a strain rate of $0{\cdot}033\ s^{-1}$ have been achieved,[170,201,202,217] which is an extraordinarily good combination of high strain and high strain rate for an aluminium alloy.

Superplastic properties of Al–Cu–Mg(–Mn)–Sc(–Zr) and Al–Mg–Sc(–Zr) alloys have been mentioned. Noticeable superplasticity in other Sc-containing Al-alloys has also been reported, such as Al–Zn–Mg(–Cu)–Sc–Zr,[169,225–228] Al–Li–Sc,[229] Al–Mg–Li–Sc–Zr,[229–234] Al–Li–Mg–Cu–Sc–Zr[235,236] and Al–Cu–Li–Sc–Zr.[233]

Precipitation hardening

Hardening by Al_3Sc precipitates

It has been noted that when Al_3Sc particles precipitate in the temperature range 250–350°C they give a significant hardness increase in the alloy. Some authors point out that Sc is a more effective precipitation hardening element per atomic fraction added than the elements that are commonly used for precipitation hardening.[121,130] (In one paper[29] it is claimed that only Au has a stronger strengthening effect than Sc.) However, the amount of Sc that can be precipitated from supersaturated solid solution is rather limited, and thus the absolute values of the hardness increase from the precipitation hardening is much lower than what is normally associated with precipitation hardened alloys. Also, the temperature regime for age hardening by precipitation of Al_3Sc is somewhere in between the temperature regimes for age hardening and solution heat treatments of common precipitation hardened alloys. This makes a combined precipitation of Al_3Sc and other strengthening precipitates unfeasible. Thus, precipitation strengthening by Al_3Sc is most feasible in alloy systems that are non-heat-treatable. The non-heat-treatable aluminium alloy systems are, according to the Aluminum Association designations, the 1xxx series (>99% pure Al), the 3xxx series (Al–Mn) and the 5xxx series (Al–Mg). The purpose of adding Sc to these alloys may be either to stabilise the microstructure of wrought semiproducts (extrusions, rolled plates, forgings, etc.) as discussed in the section on 'Recrystallisation resistance' above, or to provide extra strength to the alloy through precipitation hardening. In the latter case, it is appropriate to consider whether the Sc-containing alloy still should be classified as non-heat-treatable. A heat treatment is applied that brings about a significant precipitation hardening. On the other hand, the hardness increase that is achieved through the heat treatment is lower than what is normally associated with heat-treatable alloy systems. Hence, even though it seems like a contradiction, one chooses to keep using the term 'non-heat-treatable' about these alloys.

Table 7 gives an overview of some mechanical properties of Sc-containing non-heat-treatable alloys that are reported in the literature. Most of the experimental work on Sc in 1xxx-types of alloys has been done on binary Al–Sc alloys with much higher purity than industrial alloys.

Strengthening mechanisms

When the precipitates are larger than a critical size, the strengthening effect is due to the Orowan-mechanism, i.e. dislocations can only pass the precipitates by looping. In this case, the strengthening effect of the particles is approximately inversely proportional to the mean particle spacing. When the precipitates can be sheared by dislocations there are a number of strengthening mechanisms that apply. It is proposed by Parker *et al.*[108] that the two major contributing mechanisms are coherency strain and anti-phase-boundary energy. In a recent detailed study of strengthening mechanisms in binary Al–Sc alloys by Marquis and colleagues,[117,118] the strengthening from shear modulus mismatch between the matrix and the precipitates is also accounted for. A qualitatively good match between theoretical strengthening and measured values is achieved in this work, both for deformation at room temperature and at 300°C.

Effect of Sc on precipitation strengthening in heat-treatable alloys

Following the AA designation system, the traditional heat-treatable Al-alloys are those that belong to the 2xxx

series (Al–Cu), 6xxx series (Al–Mg–Si) and 7xxx series (Al–Zn–Mg). Al–Li alloys should also be mentioned. Several investigations have been carried out in order to clarify the effects of Sc on the precipitation behaviour in these alloy systems.

Al–Cu alloys

The precipitation sequence in Al–Cu alloys is often described as follows:

Supersaturated solid solution→GP-zones→θ''→θ'→θ(Al_2Cu)

The highest strength is normally achieved when the θ'' or θ' precipitates are predominant. Typical precipitation heat treatment temperatures for Al–Cu alloys are in the range 160–190°C,[238] which is considerably lower than the typical precipitation temperature for Al_3Sc. Comparisons of the aging responses of Al–Cu and Al–Cu–Sc alloys at 150 and 200°C indicate that there is no noticeable effect of Sc on the precipitation kinetics of θ'.[153] It is observed that the θ' precipitates may nucleate on Al_3Sc particles.[153] At 300°C, it is observed that θ' particles are somewhat smaller in Al–Cu–Sc alloys than in Al–Cu alloys.[156]

Al–Mg–Si alloys

The following precipitation sequence is commonly reported for Al–Mg–Si alloys:

Supersaturated solid solution→GP-zones→β''→β'→β (Mg_2Si)

For peak aged alloys, the predominant precipitate type is β'', for which the stoichiometric composition has recently been resolved to be Mg_5Si_6.[239] Temperatures in the range 160–205°C are typically used for precipitation hardening of these alloys.[238] Adding both 0·3 wt-%Sc and 0·1 wt-%Zr to an Al–0·6 wt-%Mg–0·65 wt-%Si alloy does not seem to alter the precipitation kinetics of β'' at 165°C. However, the hardness increase because of precipitation hardening appears to be smaller in the Sc+Zr-containing alloy.[240] In another investigation, additions of 0·1 wt-%Sc, 0·15 wt-%Sc, 0·2 wt-%Sc, 0·4 wt-%Sc and 0·2 wt-%Sc+0·1 wt-%Zr were made to an Al–0·8 wt-%Mg–0·7 wt-%Si alloy.[241] Here, it was also observed that the precipitation kinetics of β'' was seemingly independent of the Sc additions (Fig. 28). TEM observations indicated that the β'' precipitates were of comparable sizes in the investigated alloys, and no interactions between Al_3Sc and β'' were observed (Fig. 29). In a third study,[242] where the effect of Sc on the precipitation in an AlMgSi–SiC metal matrix composite was investigated, there also does not seem to be any effect on the precipitation kinetics. However, contrary to the findings of Ref. 240, it is reported that the Sc addition leads to a higher hardness increase than in the corresponding Sc free alloy.

Al–Mg–Zn alloys

For these alloys, the following precipitation sequence is often ascribed:

Table 7 Mechanical properties in non-heat-treatable Al-alloys with Sc

Reference	Alloy, wt-%	YS, MPa	UTS, MPa	Note
1xxx alloys				
171	0·00Sc	15	48	Cast material, aged 288°C/8 h
	0·23Sc	159	185	Cast material, aged 288°C/8 h
	0·38Sc	199	220	Cast material, aged 288°C/8 h
	0·00Sc	14	49	Cold rolled material (89%), aged 288°C/8 h
	0·23Sc	198	208	Cold rolled material (89%), aged 288°C/8 h
	0·38Sc	240	264	Cold rolled material (89%), aged 288°C/8 h
	0·00Sc	8	34	Cold rolled material, quenched from 649°C, aged 288°C/8 h
	0·23Sc	147	157	Cold rolled material, quenched from 649°C, aged 288°C/8 h
	0·38Sc	193	199	Cold rolled material, quenched from 649°C, aged 288°C/8 h
121	0·5Sc	160	–	Forged material, quenched from 635°C, aged 250°C/50 h
23	0·5Sc	298	319	Hot rolled 288°C, cold rolled 69–81%, aged 288°C/4 h
112	0·1Sc	132	166	Hot + cold rolled material, quenched from 630°C, aged 320°C/13·3 h
148	0·2Sc	138	–	Cast material, aged 300°C/10 h, compression test
159	0·4Sc	196	–	Cast material, aged 300°C/10 h, compression test
117, 118	0·3Sc	209	–	Cast material, quenched from 648°C, aged 300°C/5 h, compression test
3xxx alloys				
171	1Mn 0·15Sc	216	221	Cold rolled material (89%), aged 288°C/8 h
	1Mn 0·5Sc	309	323	Cold rolled material (89%), aged 288°C/8 h
186	0·5Mn 0·2Mg 0·26Sc 0·15Zr	162	201	Extruded material, solutionised 600°C, aged 250°C
5xxx alloys				
171	1Mg	43	111	Cold rolled material (89%), aged 288°C/8 h
	1Mg 0·3Sc	288	303	Cold rolled material (89%), aged 288°C/8 h
	5·3Mg	147	259	Cold rolled material (50%) w/intermediate anneals at 343°C, aged 288°C/8 h
	5·3Mg 0·3Sc	368	401	Cold rolled material (50%) w/intermediate anneals at 343°C, aged 288°C/8 h
23	2Mg 0·5Sc	376	401	Hot rolled 288°C, cold rolled 69–81%, aged 288°C/4 h
	4Mg 0·5Sc	414	460	
	6Mg 0·5Sc	433	503	
237	4Mg 1Sc	420	525	Cold rolled material (83%), aged 320°C/1 h
148	4Mg 0·2Sc	194	–	Cast material, aged 300°C/10 h, compression test

Tensile test data except where noted. YS, yield strength; UTS, ultimate tensile strength.

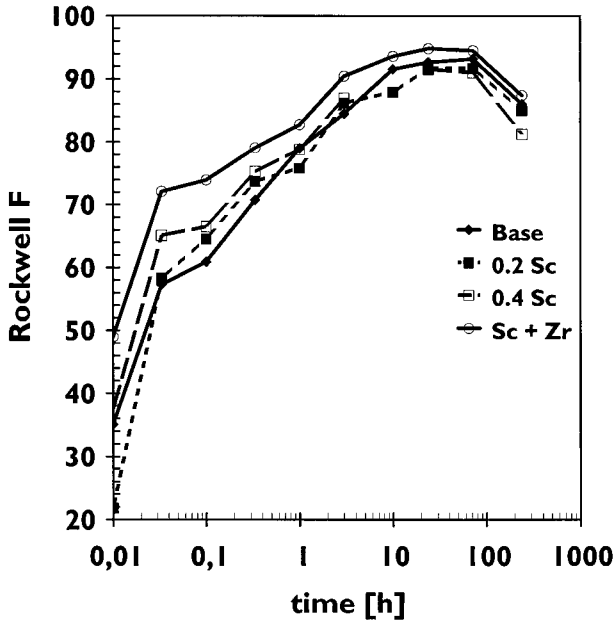

28 Age hardening response at 175°C for Al–0·8 wt-%Mg–0·7 wt-%Si alloy (Base) with additions of 0·2 wt-%Sc, 0·4 wt-%Sc and 0·2 wt-%Sc + 0·1 wt-%Zr: from Ref. 241

Supersaturated solid solution→GP-zones→η'→η (Zn_2Mg)

The maximum hardness is normally achieved when the η' precipitates are predominant. Common precipitation hardening temperatures are in the range 95–180°C, and a two-step precipitation heat treatment within this temperature regime is often used.[238] It has been observed in some investigations that Sc and Sc + Zr additions to Al–Mg–Zn alloys slow down the precipitation of η' somewhat.[243] Other investigations find that there is no effect of Sc on the precipitation behaviour of η',[244,245] and yet others report that Sc additions significantly speed up the precipitation of η'.[246] In Ref. 247, it is found that an Sc addition leads to coarser η' precipitates and it is claimed that this gives an improved ductility of the alloy. The strength-loss associated with larger particle size is reported to be counterbalanced by strengthening from Al_3Sc precipitates.

Al–Li alloys

The precipitation sequence in binary Al–Li alloys is apparently simple:

Supersaturated solid solution→δ'→δ (AlLi)

where δ' is the metastable Al_3Li phase which, just like Al_3Sc, has the $L1_2$ type of atomic arrangement. The typical temperature regime for precipitation of δ', which is the strengthening phase in this system, is approx. 150–200°C. A comparison of the age hardening response of an Al–2·6 wt-%Li and an Al–2·4 wt-%Li–0·19 wt-%Sc alloy at 180°C[248] and 200°C[161] indicates that the onset of δ' precipitation is not altered by the presence of Sc. The hardness curves for the two alloys are practically identical at 200°C, whereas at 180°C, the peak hardness level is slightly higher in the Al–Li than the Al–Li–Sc alloy. DSC measurements at constant heating rates indicate that the addition of Sc to an Al–Li alloys increases the activation energy for δ' precipitation and moves the exothermic peak associated with δ' precipitation to a higher temperature.[248] For specimens aged at either 180°C or 200°C, TEM observations reveal that the δ' precipitates are much smaller in the Sc containing alloy than in binary Al–Li, both in the peak aged condition and in the overaged condition.[161,248] Addition of Sc has also been observed to reduce the size of δ' precipitates in other Al–Li based alloys.[249–251] In an Al–Li–Cu–Zr alloy, an addition of Sc has been reported to slow down the homogeneous precipitation of δ'.[252,253] It has been claimed that Sc reduces the quench sensitivity and delays room temperature aging of Al–Li based alloys.[254–256]

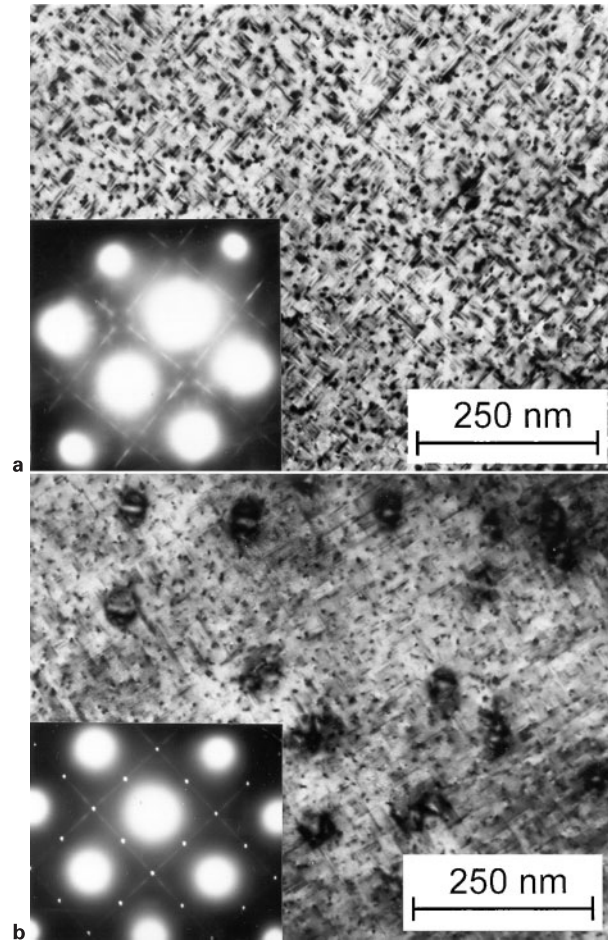

29 TEM images of *a* β'' precipitates in Al–0·8 wt-%Mg–0·7 wt-%Si alloy and *b* β'' and $Al_3(Sc_{1-x}Zr_x)$ in a similar alloy with addition of 0·2 wt-%Sc + 0·1 wt-%Zr: from Ref. 241

When present in the microstructure before the precipitation of δ', the Al_3Sc precipitates may act as effective nucleation sites for δ'. The resulting precipitates are spheres of δ' with a core of Al_3Sc.[161,249,252–255,257–261]

Corrosion resistance

An appreciable amount of data is available on the effects of Sc on the corrosion behaviour of wrought Al-alloys. Some of these effects are apparently derived from the effects of Sc on the microstructure of the alloys. It has been reported that an addition of Sc increases the corrosion potential (makes it less negative) in pure Al,[262–264] in Al–Zn alloys,[265,266] Al–Mg alloys,[267] Al–Zn–Mg–Cu alloys,[264,268] Al–Cu–Mg–Mn alloys[264] and in Al–Cu–Li–Mg–Ag alloys.[264] Even though Sc also has been reported to decrease the corrosion potential in

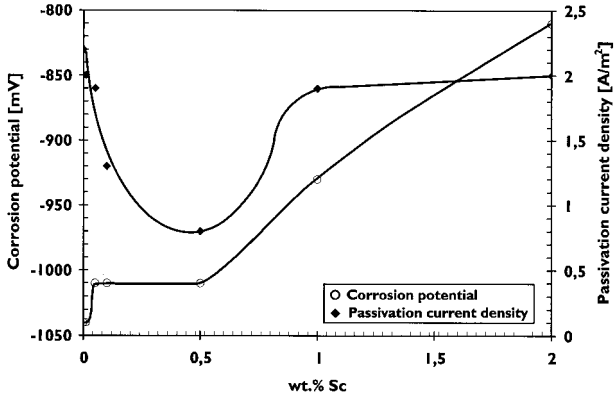

30 Observed variations in corrosion potential and passivation current densities with Sc content in binary Al–Sc alloys: based on data from Ref. 263

Al–Mg alloys,[269,270] it seems that the general trend is that adding Sc to an alloy makes it slightly more noble. The change in corrosion potential is much more pronounced when Sc is added in amounts larger than the eutectic composition,[263] i.e. there is a considerable contribution from primary or eutectic Al_3Sc to the overall potential. It has also been demonstrated that the change in corrosion potential caused by Sc can depend on the heat treatment applied to the alloy.[267,268]

Even though the corrosion potential is an essential parameter in establishing the corrosion behaviour of an alloy, an increase in the corrosion potential does not necessarily imply an improved self-corrosion resistance. However, measurements of corrosion rates and passivation current densities strongly suggest that the self-corrosion resistance in general is considerably improved when Sc is added to wrought Al-alloys.[263,264,267] Some observed variations in corrosion potential and passivation current densities with Sc content in binary Al–Sc alloys are plotted in Fig. 30.

Material failure in corrosive environments is often due to localised corrosion attacks, which may propagate rapidly even though the bulk material has a good resistance against general corrosion. It has been pointed out that hypereutectic additions of Sc may lead to microgalvanic corrosion beside primary Al_3Sc particles.[264] In Al–Mg alloys, grain boundary precipitation of Al_8Mg_5 can lead to localised corrosion attacks such as intergranular corrosion (IGC), exfoliation corrosion (EC) and stress corrosion cracking (SCC). In wrought material such precipitation may occur in the 60–180°C temperature regime, and heating in this temperature range is referred to as 'sensitation'. An Al–Mg–Sc alloy was found to be immune against intergranular corrosion and have moderate susceptibility to exfoliation corrosion after annealing at 350°C.[271] After sensitation heat treatments, severe IGC and EC was observed, but not quite as severe as in a corresponding alloy without Sc. As for SCC, the Al–Mg–Sc alloy was found to be highly resistant.[271] In another study, it was found that addition of 0·56 wt-%Sc reduces the SCC susceptibility of an Al–6·8 wt-%Mg alloy in the as-rolled state and after annealing at 250°C, whereas in a sensitised specimen, the SCC susceptibility is somewhat increased by the Sc addition.[272] A third investigation found that Sc has no measurable detrimental effect on the SCC susceptibility of sensitised Al–5%Mg–0·15%Zr alloy.[273] SCC is also a severe problem in high strength Al–Zn–Mg–Cu alloys. It has been shown that small Sc additions are effective in reducing the SCC sensitivity of these alloys.[244,246,268,274]

Use of Sc-containing Al alloys

A systematic development of Sc-containing aluminium alloys took place in the former USSR in the 1980s, and the interest for Sc as an alloying element in aluminium alloys hit the western world approximately 10 years later. Even though a number of improvements in Al alloys achieved by Sc addition have been demonstrated, the current uses of such alloys are very limited. This is related to the very high price of scandium.

In Russia, some parts of military aircraft are made of Sc-containing Al–Li alloys. In the western world, the main usage of Sc-containing alloys is for sports equipment. Ashurst Technology and Kaiser Aluminum developed a Sc-containing 7xxx alloy for baseball and softball bats, which was introduced to the American market in 1997 by Easton. Alcoa soon followed with a Sc-containing alloy for a competing brand of bats, Louisville Slugger. Since then, several new and improved Sc-containing alloys for bats have been introduced to the market. The purpose of adding Sc is to increase the yield strength of the alloy, allowing for a down-gauging of the wall thickness, which in turn gives a stronger 'spring-' or 'trampoline-' effect when the ball hits the bat.

Shortly after the introduction of the Sc containing bats, Easton also launched Sc-containing 7xxx tubing for bicycle frames. Just as in the bats, Sc increases the yield strength of the alloy, allowing for down-gauging of tube wall thickness and a corresponding weight reduction of the bicycle frame. An Italian manufacturer of bicycle tubing, Dedacciai, also delivers tubes in a Sc-containing 7xxx alloy.

Other sports equipment made from Sc-containing aluminium alloys includes lacrosse sticks and tent poles. Smith and Wesson has also introduced a series of handguns where the frame is made from a Sc-containing Al alloy.

A common factor for the items mentioned above is that the material cost is only a minor part of the total manufacturing cost of the end product, and also that these products are aimed at a group of customers that have a certain awareness of new materials. Both baseball bats and bicycle frames have been marketed as 'scandium alloy' even though the Sc content is much lower than 1%.

Currently, Al–Sc master alloys for the production of Sc-containing Al alloys are available at a price that corresponds to US$ 2000 per kg of Sc. This means that if one wants to add 0·2 wt-%Sc to an alloy, which is a fairly common content, one also increases the price of the alloy by US$ 4 per kg alloy. Depending on the alloy type Sc is added to, this represents a tripling or quadrupling of the price of the alloy. There are not many existing products where such an increase in material cost can be justified. In order to see a widespread use of Sc in high-volume products, the Sc price has to come down considerably. Actually, the price of adding Sc to Al alloys has gone down by a factor 3–10 over the last 10–15 years, and substantial price reductions are also expected in the future.

The current production of Al–Sc master alloys is based upon, and will continue to be based upon for the foreseeable future, the reduction of Sc_2O_3 or other Sc compounds directly in molten aluminium. It is not necessary, as many tend to believe, to take the route via metallic Sc. Thus, the price of Al–Sc master alloy is governed by the price of Sc_2O_3 or other Sc compounds in question, and not by the price of metallic scandium. The Sc_2O_3 which is the main source for today's Al–Sc master alloy production comes from stockpiles in the former USSR. These stockpiles will be exhausted within a few years, and new, reliable sources of Sc_2O_3 or other Sc compound production are sought. It turns out that the most economically viable option that has been disclosed so far is the processing of Red Mud from the Bayer process of extracting alumina from bauxite. Scandium is enriched in the Red Mud, and is extracted from a Red Mud aqueous slurry by selective leaching, subsequent ion-exchange procedure and finally a liquid–liquid extraction procedure. It is not required to build a separate 'Sc factory' to do this, but rather build an 'add-on' to existing Bayer process plants. Such a process route is expected to bring down the price of Sc_2O_3 considerably, which in turn means that Al–Sc master alloy price should drop accordingly. Preliminary analyses suggest a price of approx. US$ 400 per kg Sc in the master alloy, which translates to an added cost of 80 cent per kilo when 0·2 wt-%Sc is added to an aluminium alloy. This is also a considerable increase in the material cost, but with such prices, one should expect to see Sc containing alloys in many more applications than what is the case at the present time.

Concluding remarks

The body of published investigations on Al-based alloys with Sc addition provides a sound basis of knowledge for metallurgists that want to look into the possibility of enhancing the performance of a wrought Al-alloy by adding Sc to it. Ternary Al–Sc–X phase diagrams are available for practically every technologically important alloying element in Al. The effect of a wide range of ternary alloying elements on the precipitation behaviour of Al_3Sc is accounted for. It has been shown that the Al_3Sc phase can be effective as a grain refiner, a dispersoid former and a precipitate hardening agent, and some of the underlying conditions for achieving the desired Al_3Sc formation have been outlined. Adding some Zr together with Sc has proven to be beneficial. It may lead to effective grain refinement at a lower Sc level, but the most prominent effect is the refinement in dispersoid distribution that can be achieved. An addition of Sc has little, if any, effect on precipitation in the 2xxx, 6xxx and 7xxx alloy systems, and some effects on the precipitation in Al–Li based alloys. With respect to corrosion behaviour, adding Sc to an Al-alloy does in general seem to make the alloy slightly more noble and to increase its self-corrosion resistance. Scandium-containing Al alloys have very few uses at the present time as a result of the high price of scandium. The price of Sc is expected to decrease significantly in the future, and this should lead to the disclosure of more applications where it is economically feasible to take advantage of the improved properties of some Sc-containing aluminium alloys.

References

1. D. R. Lide: 'CRC handbook of chemistry and physics', 71st edn, 4–29; 1990, Boston, USA, CRC Press.
2. E. M. Savitsky, V. F. Terehova, I. V. Burov and O. P. Naumkin: Proc. Fourth Conf. on 'Rare earth research', Phoenix, Arizona, USA, April 1964, 409–420.
3. E. M. Savitskii, V. F. Terekhova, I. V. Burov, O. P. Naumkin and I. A. Markova: *Inorg. Mater.*, 1965, **1**, 1503–1512.
4. O. P. Naumkin, V. T. Terekhova and E. M. Savitskiy: *Russ. Metall.*, 1965, (4), 128–136.
5. W. G. Moffatt: 'The handbook of binary phase diagrams'; 1981, Schenectady, NY, USA, General Electric Co.
6. E. A. Brandes (ed.): 'Smithells metals reference book', 6th edn; 1983, London, UK, Butterworths.
7. R. P. Elliott and F. A. Shunk: *Bull. Alloy Phase Diagrams*, 1981, **2**, (2), 222–223.
8. K. A. Gschneider, Jr and F. W. Calderwood: *Bull. Alloy Phase Diagrams*, 1989, **10**, 34–36.
9. H. Okamoto: *J. Phase Equil.*, 1991, **12**, 612–613.
10. J. L. Murray: *J. Phase Equil.*, 1998, **19**, 380–384.
11. M. E. Drits, E. S. Kadaner, T. V. Dobatkina and N. I. Turkina: *Russ. Metall.*, 1973, (4), 152–154.
12. S.-I. Fujikawa, M. Sugaya, H. Takei and K.-I. Hirano: *J. Less-Common Met.*, 1979, **63**, 87–97.
13. N. Blake and M. A. Hopkins: *J. Mater. Sci.*, 1985, **20**, 2861–2867.
14. V. I. Kononenko and S. V. Golubev: *Russ. Metall.*, 1990, (2), 193–195.
15. T. B. Massalski, J. L. Murray, L. H. Bennett and H. Baker (eds.): 'Binary alloy phase diagrams'; 1986, Metals Park, OH, USA, ASM.
16. G. Cacciamani, P. Riani, G. Borzone, N. Parodi, A. Saccone, R. Ferro, A. Pisch and R. Schmid-Fetzer: *Intermetallics*, 1999, **7**, 101–108.
17. H. Okamoto: *J. Phase Equil.*, 2000, **21**, 310.
18. A. F. Norman, P. B. Pragnell and R. S. McEwen: *Acta Mater.*, 1998, **46**, 5715–5732.
19. I. N. Pyagai and A. V. Vakhobov: *Russ. Metall.*, 1990, (5), 50–52.
20. C. L. Fu: *J. Mater. Res.*, 1990, **5**, 971–979.
21. X. Lu and Y. Wang: *Calphad*, 2002, **26**, 555–561.
22. R. R. Sawtell and J. W. Morris, Jr: Proc. 'Dispersion strengthened aluminium alloys', Phoenix, Arizona, USA, January 1988, 409–420.
23. R. R. Sawtell and C. L. Jensen: *Metall. Trans. A*, 1990, **21A**, 421–430.
24. L. A. Willey: Unpublished research, Alcoa, 1970. Data points are extracted from Ref. 10.
25. N. I. Turkina and V. I. Kuzmina: *Russ. Metall.*, 1976, (4), 179–183.
26. T. Torma, E. Kovács-Cseténi, I. Vitányi, M. Butova and J. Stepanov: Proc. 6th Int. Symp. on 'High purity materials in science and technology', Akademie der Wissenschaften der DDR, Dresden, Germany, May 1985, 388–389.
27. A. L. Berezina, V. A. Volkov, B. P. Domashnikov and K. V. Chuistov: *Metallofizika*, 1987, **9**, (5), 43–47.
28. H.-H. Jo: *J. Korean Inst. Metals*, 1990, **28**, 499–504.
29. H.-H. Jo and S.-I. Fujikawa: *Mater. Sci. Eng.*, 1993, **A 171**, 151–161.
30. S. Celotto and T. J. Bastow: *Philos. Mag. A*, 2000, **80**, 1111–1125.
31. J. Røyset and N. Ryum: submitted to *Mater. Sci. Eng.*
32. M. E. Drits, L. S. Toropova, Yu. G. Bykov, F. L. Gushchina, V. I. Elagin and Yu. A. Filatov: *Russ. Metall.*, 1983, (1), 150–153.
33. L. S. Toropova, D. G. Eskin, M. L. Kharakterova and T. V. Dobatkina: 'Advanced aluminum alloys containing scandium: structure and properties'; 1998, Amsterdam, The Netherlands, Gordon and Breach Science Publishers.
34. V. V. Cherkasov, P. P. Pobezhimov, L. P. Nefedova, E. V. Belov and G. M. Kuznetsov: *Met. Sci. Heat Treat.*, 1996, (6), 268–270.
35. Kh. O. Odinaev, I. N. Ganiev, V. V. Kinzhibalo and B. Ya. Kotur: *Dokl. Akad. Nauk. Tadzh. SSR*, 1989, **32**, 37–38.
36. Kh. O. Odinaev, I. N. Ganiev and A. V. Vakhobov: *Russ. Metall.*, 1991, (4) 200–203.
37. J. Gröbner, R. Schmid-Fetzer, A. Pisch, G. Cacciamani, P. Riani, N. Parodi, G. Borzone, A. Saccone and R. Ferro: *Z. Metallkd.*, 1999, **90**, 872–880.
38. E. A. Marquis and D. N. Seidman: *Microsc. Microanal.*, 2002, **8**, (Suppl. 2), 1100CD–1101CD.
39. A. Pisch, J. Gröbner and R. Schmid-Fetzer: *Mater. Sci. Eng. A*, 2000, **A 289**, 123–129.

40. C. Xia, F. Zeng and Y. Gu: *Trans. Nonferrous Met. Soc. China*, 2003, **13**, 1124–1127.
41. M. Yu. Teslyuk and V. S. Protasov: *Sov. Phys. Crystallogr.*, 1966, **10**, 470–471.
42. M. L. Kharakterova and T. V. Dobatkina: *Russ. Metall.*, 1988, (6), 175–178.
43. M. L. Kharakterova: *Russ. Metall.*, 1991, (4), 195–199.
44. L. S. Toropova, M. L. Kharakterova and D. G. Eskin: *Russ. Metall.*, 1992, (3), 194–199.
45. P. Riani, L. Arrighi, R. Marazza, D. Mazzone, G. Zanicchi and R. Ferro: *J. Phase Equil. Diff.*, 2004, **25**, 22–52.
46. A. T. Tyvanchuk, T. I. Yanson, B. Ya. Kotur, O. S. Zarechnyuk and M. L. Kharakterova: *Russ. Metall.*, 1988, (4), 190–192.
47. L. L. Rokhlin, T. V. Dobatkina and M. L. Kharakterova: *Powder Metall. Met. Ceram.*, 1997, **36**.
48. A. Z. Ikromov, I. N. Ganiev and V. V. Kinzhibalo: *Dokl. Akad. Nauk. Tadzh. SSR*, 1990, (6), 391–392.
49. I. N. Ganiev, A. Z. Ikromov and V. G. Khudoiberdiev: *Russ. Metall.*, 1995, (3), 125–127.
50. I. N. Fridlyander, L. L. Rokhlin, T. V. Dobatkina and N. I. Nikitina: *Met. Sci. Heat Treat.*, 1993, (10), 567–571.
51. I. N. Fridlyander, L. L. Rokhlin, T. V. Dobatkina, V. V. Kinzhibalo and A. T. Tyvanchuk: *Russ. Metall.*, 1998, (1), 161–166.
52. R. A. Emigh, E. L. Bradley and J. W. Morris, Jr: in 'Light-weight alloys for aerospace applications II', (ed. E. W. Lee and N. J. Kim), 27–43; 1991, TMS.
53. L. S. Toropova, A. N. Kamardinkin, V. V. Kindzhibalo and A. T. Tyvanchuk: *Phys. Met. Metall.*, 1990, **70**, (6), 106–110.
54. A. N. Kamardinkin, T. V. Dobatkina and T. D. Rostova: *Russ. Metall.*, 1991, (4), 216–218.
55. L. S. Torodskaya, T. V. Dobatkina and A. N. Kamardinkin: *Russ. Metall.*, 1992, (5), 128–131.
56. E. M. Sokolovskaya, E. F. Kazakova, E. I. Poddyakova and A. A. Ezhov: *Met. Sci. Heat Treat.*, 1997, (5), 211–213.
57. Y. Harada and D. C. Dunand: *Mater. Sci. Eng.*, 2002, **A 329–331**, 686–695.
58. N. E. Drits, L. S. Toropova and F. L. Gushchina: *Russ. Metall.*, 1984, (4), 229–232.
59. E. M. Sokolovskaya, E. F. Kazakova, V. A. Alikhanov and E. V. Zhuravleva: *Moscow Univ. Chem. Bull.*, 1997, **52**, (5), 70–72.
60. E. M. Sokolovskaya, E. F. Kazakova and E. I. Poddyakova: *Met. Sci. Heat Treat.*, 1989, (11), 837–839.
61. G. M. Cheldieva, E. F. Kazakova, E. M. Sokolovskaya and N. I. Kaloev: *Russ. Metall.*, 1990, (6), 87–90.
62. E. M. Sokolovskaya, E. F. Kazakova and O. D.-S. Kendivan: *Russ. Metall.*, 1998, (4), 135–137.
63. N. G. Bukhanko, E. F. Kazakova and E. M. Sokolovskaya: *Russ. Metall.*, 2001, (4), 425–431.
64. E. D. Trubnyakova, O. I. Bodak, I. N. Ganiev and A. V. Vakhobov: *Russ. Metall.*, 1987, (3), 219–222.
65. I. N. Fridlyander and L. V. Molchanova: *Russ. Metall.*, 2003, (5), 476–480.
66. R. A. Altynbaev, S. Kh. Khairidinov and A. V. Vakhobov: *Russ. Metall.*, 1987, (4) 194–196.
67. J. C. Schuster and J. Bauer: *J. Less-Common Met.*, 1985, **109**, 345–350.
68. L. L. Rokhlin, A. S. Fridman, T. V. Dobatkina and D. G. Eskin: *Russ. Metall.*, 1991, (6), 146–148.
69. A. S. Fridman, T. V. Dobatkina and E. V. Muratova: *Russ. Metall.*, 1992, (1), 207–209.
70. C. Xia, F. Zeng and Y. Gu: *Trans. Nonferrous Met. Soc. China*, 2003, **13**, 546–552.
71. F. Zeng, C. Xia and Y. Gu: *J. Alloys Comp.*, 2004, **363**, 175–181.
72. L. L. Rokhlin, T. V. Dobatkina, N. R. Bochvar and E. V. Lysova: *J. Alloys Comp.*, 2004, **367**, 10–16.
73. T. V. Dobatkina, A. S. Fridman and E. V. Muratova: *Russ. Metall.*, 1992, (5), 125–127.
74. I. N. Fridlyander, L. L. Rokhlin, N. R. Bochvar, E. V. Lysova and O. V. Boteva: *Russ. Metall.*, 2001, (6), 661–666.
75. V. N. Rechkin, L. K. Lamikhov and T. I. Samsonova: *Sov. Phys. Crystallogr.*, 1964, **9**, 325–327.
76. I. I. Zalutskii and P. I. Kripyakevich: *Sov. Phys. Crystallogr.*, 1967, **12**, 341–343.
77. T. J. Bastow, C. T. Forwood, M. A. Gibson and M. E. Smith: *Phys. Rev. B*, 1998, **58**, 2988–2997.
78. K. Fukunaga, M. Kolbe, K. Yamada and Y. Miura: *Mater. Sci. Eng.*, 1997, **A 234–236**, 594–597.
79. E. P. George, J. A. Horton, W. D. Porter and J. H. Schneibel: *J. Mater. Res.*, 1990, **5**, 1639–1648.
80. E. P. George, D. P. Pope, C. L. Fu and J. H. Schneibel: *ISIJ Int.*, 1991, **31**, 1063–1075.
81. Y. Harada and D. C. Dunand: *Acta Mater.*, 2000, **48**, 3477–3487.
82. J. H. Schneibel and E. P. George: *Scripta Metall. Mater.*, 1990, **24**, 1069–1074.
83. J. H. Schneibel and P. M. Hazzledine: *Mater. Res. Soc. Symp. Proc.*, 1991, **213**, 323–328.
84. J. H. Schneibel and P. M. Hazzledine: *J. Mater. Res.*, 1992, **7**, 868–875.
85. C. J. Sparks, E. D. Specht, G. E. Ice, P. Zschack and J. Schneibel: *Mater. Res. Soc. Symp. Proc.*, 1991, **213**, 363–368.
86. J. Tarnacki and Y.-W. Kim: *Scripta Metall. Mater.*, 1989, **23**, 1063–1068.
87. M. Asta, V. Ozolins and C. Woodward: *JOM*, 2001, **53**, (9), 16–19.
88. M. E. Drits, L. S. Toropova, F. L. Gushchina and S. G. Fedotov: *Sov. Non-Ferrous Met. Res.*, 1984, **12**, 83–85.
89. Y. Harada and D. C. Dunand: *Scripta Mater.*, 2003, **48**, 219–222.
90. C. Woodward, M. Asta, G. Kresse and J. Hafner: *Phys. Rev. B*, 2001, **63**, 094103-1-6.
91. J.-H. Xu and A. J. Freeman: *Phys. Rev. B*, 1990, **41**, 12553–12561.
92. M. F. Bartholomeusz and J. A. Wert: *Acta Metall. Mater.*, 1992, **40**, 673–682.
93. G. Bester and M. Fähnle: *J. Phys. Condens. Matter*, 2001, **13**, 11551–11565.
94. C. L. Fu and M. H. Yoo: Proc. 'Ordered intermetallics – physical metallurgy and mechanical behavior', Irsee, Germany, June 1991, 155–164.
95. K. Fukunaga, T. Shouji and Y. Miura: *Mater. Sci. Eng.*, 1997, **A 239–240**, 202–205.
96. D. P. Pope: Proc. 'Ordered intermetallics – physical metallurgy and mechanical behavior', Irsee, Germany, June 1991, 143–153.
97. J.-S. Wang: *Acta Mater.*, 1998, **46**, 2663–2674.
98. M. H. Yoo and C. L. Fu: *Mater. Sci. Eng.*, 1992, **A 153**, 470–478.
99. R. W. Hyland, Jr and R. C. Stiffler: *Scripta Metall. Mater.*, 1991, **25**, 473–477.
100. I. G. Brodova, I. V. Polents, O. A. Korzhavina, P. S. Popel', I. P. Korshunov and V. O. Esin: *Melts*, 1992, **4**, 392–397.
101. I. G. Brodova, O. A. Chikova, I. V. Polents, P. S. Popel' and V. O. Esin: *Casting Processes*, 1992, **1**, (2), 158–160.
102. I. G. Brodova, D. V. Bashlikov and I. V. Polents: *Mater. Sci. Forum*, 1998, **269–272**, 589–594.
103. K. B. Hyde, A. F. Norman and P. B. Pragnell: *Mater. Sci. Forum*, 2000, **331–337**, 1013–1018.
104. K. B. Hyde, A. F. Norman and P. B. Pragnell: *Acta Mater.*, 2001, **49**, 1327–1337.
105. J. Røyset and N. Ryum: Proc. 6th Int. Conf. on 'Aluminum alloys', Toyohashi, Japan, July 1998, 793–798.
106. V. I. Elagin, V. V. Zakharov and T. D. Rostova: *Met. Sci. Heat Treat.*, 1993, (6), 317–319.
107. R. W. Hyland, Jr: *Metall. Trans. A*, 1992, **23A**, 1947–1955.
108. B. A. Parker, Z. F. Zhou and P. Nolle: *J. Mater. Sci.*, 1995, **30**, 452–458.
109. C. L. Rohrer, M. D. Asta, S. M. Foiles and R. W. Hyland, Jr: *Mater. Res. Soc. Symp. Proc.*, 1996, **398**, 477–482.
110. G. M. Novotny and A. J. Ardell: *Mater. Sci. Eng.*, 2001, **A 318**, 144–154.
111. J. D. Robson, M. J. Jones and P. B. Pragnell: *Acta Mater.*, 2003, **51**, 1453–1468.
112. C. Tan, Z. Zheng and B. Wang: Proc. 3rd Int. Conf. on 'Aluminium alloys', Vol. I, NTH, Trondheim, Norway, June 1992, 290–294.
113. M. Nakayama, A. Furuta and Y. Miura: *Mater. Trans., JIM*, 1997, **38**, 852–857.
114. E. A. Marquis and D. N. Seidman: *Acta Mater.*, 2001, **49**, 1909–1919.
115. M. J. Jones and F. J. Humphreys: *Acta Mater.*, 2003, **51**, 2149–2159.
116. E. A. Marquis, D. N. Seidman and D. C. Dunand: in 'Creep deformation: fundamentals and applications', (ed. R. S. Mishra, J. C. Earthman and S. V. Raj), 299–308; 2002, TMS.
117. D. N. Seidman, E. A. Marquis and D. C. Dunand: *Acta Mater.*, 2002, **50**, 4021–4035.
118. E. A. Marquis, D. N. Seidman and D. C. Dunand: *Acta Mater.*, 2003, **51**, 285–287.
119. M. E. Drits, L. S. Toropova, U. G. Bikov and G. K. Anastaseva: Proc. 'Diffusion in metals and alloys', Tihany, Hungary, August–September 1982, 616–623.
120. V. I. Elagin, V. V. Zakharov and T. D. Rostova: *Met. Sci. Heat Treat.*, 1983, (7), 546–549.

121. M. Ye. Drits, L. B. Ber, Yu. G. Bykov, L. S. Toropova and G. K. Anastaseva: *Phys. Met. Metall.*, 1984, **57**, (6), 118–126.
122. M. E. Drits, L. S. Toropova and Yu. G. Bykov: *Sov. Non-Ferrous Met. Res.*, 1985, **13**, 309–314.
123. V. I. Yelagin, V. V. Zakharov, S. G. Pavlenko and T. D. Rostova: *Phys. Met. Metall.*, 1985, **60**, (1), 88–92.
124. N. Sano, Y. Hasegawa, K. Hono, H. Jo, K. Hirano, H. W. Pickering and T. Sakurai: *Journal de Physique*, 1987, **48**, C6, 337–342.
125. N. Sano, H.-H. Jo, K.-I. Hirano and T. Sakurai: *J. Jpn Inst. Metals*, 1989, **39**, 444–450.
126. N. Sano, H. Jo, K. Hirano and T. Sakurai: Proc. Second Int. Conf. on 'Aluminium alloys', Beijing, China, October 1990, 549–554.
127. Y. Miura, M. Nakayama and A. Furuta: Proc. 'Aspects of high temperature deformation and fracture in crystalline materials', Nagoya, Japan, July 1993, 255–262.
128. Y. W. Riddle and T. H. Sanders, Jr: *Mater. Sci. Forum*, 2000, **331–337**, 939–944.
129. Y. W. Riddle, M. McIntosh and T. H. Sanders, Jr: in 'Lightweight alloys for aerospace application VI', (ed. K. Jata, E. W. Lee, W. Frazier and N. J. Kim), 25–39; 2001, TMS.
130. M. E. Drits, J. Dutkiewicz, L. S. Toropova and J. Salawa: *Crystal Res. Technol.*, 1984, **19**, 1325–1330.
131. Y. W. Riddle: MSc thesis, Georgia Tech, GA, USA, 1998.
132. T. J. Bastow and S. Celotto: *Mater. Sci. Eng.*, 2003, **C 23**, 757–762.
133. M. C. Carroll, M. J. Mills, G. S. Daehn, P. I. Gouma, M. F. Savage and B. R. Dunbar: in 'Automotive Alloys 1999', (ed. S. Das), 239–246; 2000, TMS.
134. E. Clouet, M. Nastar and C. Sigli: *Phys. Rev. B*, 2004, **69**, 064109-1-14.
135. V. V. Zakharov: *Met. Sci. Heat Treat.*, 1997, (2), 61–66.
136. J. W. Christian: 'The theory of transformation in metals and alloys', 2nd edn; 1975, Pergamon Press Ltd.
137. A. L. Berezina, V. A. Volkov, B. P. Domashnikov, S. V. Ivanov and K. V. Chuistov: *Phys. Metals*, 1990, **10**, 296–304.
138. S.-I. Fujikawa and S. Sakauchi: Proc. 6th Int. Conf. on 'Aluminum alloys', Toyohashi, Japan, July 1998, 805–810.
139. Y. S. Touloukian, R. K. Kirby, R. E. Taylor and P. D. Desai (eds.): 'Thermal expansion: metallic elements and alloys'; 1975, New York, Plenum.
140. J. Røyset and N. Ryum: submitted to *Scripta Mater.*
141. R. O. Simmons and R. W. Balluffi: *Phys. Rev.*, 1960, **117**, 52–61.
142. M. Očko, E. Babić, R. Krsmik, E. Girt and B. Leontić: *J. Phys. F: Metals Phys.*, 1976, **6**, 703–707.
143. M. J. Jones and F. J. Humphreys: Proc. First Joint Int. Conf. on 'Recrystallization and grain growth', Aachen, Germany, August 2001, Springer Verlag, 1287–1292.
144. S. Iwamura, M. Nakayama and Y. Miura: *Mater. Sci. Forum*, 2002, **396–402**, 1151–1156.
145. S. Iwamura and Y. Miura: *Acta Mater.*, 2004, **52**, 591–600.
146. M. Asta, S. M. Foiles and A. A. Quong: *Phys. Rev. B*, 1998, **57**, 11265–11275.
147. R. W. Hyland, Jr, M. Asta, S. M. Foiles and C. L. Rohrer: *Acta Mater.*, 1998, **46**, 3667–3678.
148. J. Røyset and N. Ryum: Proc. 4th Int. Conf. on 'Aluminium alloys', Vol. I, Atlanta, GA, USA, September 1994, 194–201.
149. M. E. Drits, L. S. Toropova, G. K. Anastaseva and G. L. Nagornichnykh: *Russ. Metall.*, 1984, (3), 192–195.
150. E. A. Marquis, D. N. Seidman and D. C. Dunand: *Acta Mater.*, 2003, **51**, 4751–4760.
151. M. E. Drits, L. S. Toropova and Yu. G. Bykov: *Met. Sci. Heat Treat.*, 1983, (7), 550–554.
152. V. V. Zakharov and T. D. Rostova: *Met. Sci. Heat Treat.*, 1995, (2), 65–69.
153. M. Nakayama and Y. Miura: Proc. 4th Int. Conf. on 'Aluminium alloys', Vol. I, Atlanta, GA, USA, September 1994, 538–545.
154. M. Nakayama and Y. Miura: *J. Jpn Inst. Light Metals*, 1996, **46**, 275–279.
155. M. Nakayama, T. Okuyama and Y. Miura: *Mater. Sci. Forum*, 2000, **331–337**, 927–932.
156. M. Nakayama, T. Okuyama and Y. Miura: Proc. 6th Int. Conf. on 'Aluminum alloys', Toyohashi, Japan, July 1998, 517–522.
157. M. L. Kharakterova, D. G. Eskin and L. S. Toropova: *Acta Metall. Mater.*, 1994, **42**, 2285–2290.
158. V. I. Elagin, V. V. Zakharov and T. D. Rostova: *Met. Sci. Heat Treat.*, 1992, (1), 37–45.
159. H. Wiik: Siv. Ing. thesis, NTH, Institute of Metallurgy, Trondheim, Norway, 1995.
160. J. Røyset, H. Hovland and N. Ryum: *Mater. Sci. Forum*, 2002, **396–402**, 619–624.
161. Y. Miura, K. Horikawa, K. Yamada and M. Nakayama: Proc. 4th Int. Conf. on 'Aluminium alloys', Vol. II, Atlanta, GA, USA, September 1994, 161–168.
162. Y. W. Riddle: PhD thesis, Georgia Tech, GA, USA, 2000.
163. B. Forbord, W. Lefebvre, F. Danoix, H. Hallem and K. Marthinsen: *Scripta Mater.*, 2004, **51**, 333–337.
164. J. D. Robson: *Acta Mater.*, 2004, **52**, 1409–1421.
165. C. B. Fuller, J. L. Murray and D. N. Seidman: submitted to *Acta Mater.*, 2004.
166. M. G. Mousavi, C. E. Cross and Ø. Grong: *Sci. Technol. Weld. Joining*, 1999, **4**, 381–388.
167. J. S. Vetrano, S. M. Bruemmer, L. M. Pawlowski and I. M. Robertson: *Mater. Sci. Eng.*, 1997, **A 238**, 101–107.
168. Y. W. Riddle and T. H. Sanders, Jr: *Mater. Sci. Forum*, 2000, **331–337**, 799–803.
169. G. M. Khan, A. O. Nikiforov, V. V. Zakharov and I. I. Novikov: *Tsvetnye Metally*, 1993, **34**, (11), 43–45.
170. Z. Horita, M. Furukawa, M. Nemoto, A. J. Barnes and T. G. Langdon: *Acta Mater.*, 2000, **48**, 3633–3640.
171. L. A. Willey: US Patent 3 619 181, 9 November 1971.
172. L. K. Lamikhov and G. V. Samsonov: *Tsvetnye Metally*, 1964, **5**, (8), 77–80.
173. A. L. Berezina, K. V. Chuistov, N. I. Kolobnev, L. B. Khokhlatova and T. A. Monastyrskaya: *Mater. Sci. Forum*, 2002, **396–402**, 741–746.
174. F. A. Fasoyinu, J. Thomson, D. Cousineau, T. Castles and M. Sahoo: Proc. 6th Int. AFS Conf. on 'Molten aluminum processing', Orlando, FL, USA, November 2001.
175. Z. Yin, Q. Pan, Y. Zhang and F. Jiang: *Mater. Sci. Eng.*, 2000, **A 280**, 151–155.
176. I. I. Novikov and O. E. Grushko: *Mater. Sci. Technol.*, 1995, **11**, 926–932.
177. D. Cousineau, M. Sahoo, P. D. Newcombe, T. Castles and F. A. Fasoyinu: Proc. 'AFS 105th casting congress', Dallas, TX, USA, April–May 2001, 157–184.
178. C. E. Cross and Ø. Grong: Proc. 6th Int. Conf. on 'Aluminum alloys', Toyohashi, Japan, July 1998, 1441–1446.
179. F. A. Costello, J. D. Robson and P. B. Prangnell: *Mater. Sci. Forum*, 2002, **396–402**, 757–762.
180. K. B. Hyde, A. F. Norman and P. B. Prangnell: *Mater. Sci. Forum*, 2002, **396–402**, 39–44.
181. M. E. Drits, S. G. Pavlenko, L. S. Toropova, Yu. G. Bukov and L. B. Ber: *Sov. Phys. Dokl.*, 1981, **26**, (3), 344–346.
182. A. M. Drits and B. A. Kopeliovich: *Russ. Metall.*, 1985, (4), 147–151.
183. V. G. Davydov, V. I. Elagin, V. V. Zakharov and T. D. Rostova: *Met. Sci. Heat Treat.*, 1996, (8), 347–352.
184. M. E. Drits, L. S. Toropova, Yu. G. Bykov, L. B. Ber and S. G. Pavlenko: *Russ. Metall.*, 1982, (1), 148–152.
185. T. D. Rostova, V. G. Davydov, V. I. Yelagin and V. V. Zakharov: *Mater. Sci. Forum*, 2000, **331–337**, 793–798.
186. Y. W. Riddle, H. Hallem and N. Ryum: *Mater. Sci. Forum*, 2002, **396–402**, 563–568.
187. J. Røyset and Y. W. Riddle: Proc. 9th Int. Conf. on 'Aluminium alloys', Brisbane, Australia, August 2004, 1210–1215.
188. A. M. Diskin, V. K. Portnoi, A. M. Drits and A. A. Alalykin: *Sov. Non-Ferrous Met. Res.*, 1986, **14**, 499–500.
189. R. R. Sawtell, P. E. Bretz and C. L. Jensen: US Patent 4 689 090, 25 August 1987.
190. G. A. Salishchev, Yu. B. Timoshenko and R. A. Saitova: Proc. Second Int. Conf. on 'Aluminium alloys', Beijing, China, October 1990, 413–415.
191. T. G. Nieh, R. Kaibyshev, L. M. Hsiung, N. Nguyen and J. Wadsworth: *Scripta Mater.*, 1997, **36**, 1011–1016.
192. T. G. Nieh, L. M. Hsiung, J. Wadsworth and R. Kaibyshev: *Acta Mater.*, 1998, **46**, 2789–2800.
193. J. S. Vetrano, C. H. Henager, Jr, M. T. Smith and S. M. Bruemmer: in 'Hot deformation of aluminum alloys II', (ed. T. R. Bieler, L. A. Lalli and S. R. MacEwen), 407–418; 1998, TMS.
194. J. S. Vetrano, C. H. Henager, Jr, S. M. Bruemmer, Y. Ge and C. H. Hamilton: in 'Superplasticity and Superplastic Forming 1998', (ed. A. K. Gosh and T. R. Bieler), 89–97; 1998, TMS.
195. V. Y. Gertsman, J. S. Vetrano, C. H. Henager, Jr and S. M. Bruemmer: Proc. First Joint Int. Conf. on 'Recrystallization and grain growth', Aachen, Germany, August 2001, Springer Verlag, 2001, 837–842.
196. Y. Xiao, C. Gao, H. Ma and S. Tian: *Trans. Nonferrous Met. Soc. China*, 2001, **11**, 235–238.

197. A. Gholinia, F. J. Humphreys and P. B. Prangnell: *Acta Mater.*, 2002, **50**, 4461–4476.
198. A. Gholinia, F. J. Humphreys and P. B. Prangnell: *Mater. Sci. Forum*, 2002, **408–412**, 1519–1524.
199. S. Komura, P. B. Berbon, M. Furukawa, Z. Horita, M. Nemoto and T. G. Langdon: *Scripta Mater.,* 1998, **38**, 1851–1856.
200. S. Komura, P. B. Berbon, A. Utsunomiya, M. Furukawa, Z. Horita, M. Nemoto and T. G. Langdon: in 'Hot deformation of aluminum alloys II', (ed. T. R. Bieler, L. A. Lalli and S. R. MacEwen), 125–138; 1998, TMS.
201. S. Komura, Z. Horita, M. Furukawa, M. Nemoto and T. G. Langdon: *J. Mater. Res.*, 2000, **15**, 2571–2576.
202. S. Komura, M. Furukawa, Z. Horita, M. Nemoto and T. G. Langdon: *Mater. Sci. Eng.*, 2001, **A 297**, 111–118.
203. S. Komura, Z. Horita, M. Furukawa, M. Nemoto and T. G. Langdon: *Metall. Mater. Trans. A*, 2001, **32A**, 707–716.
204. Z. Horita, M. Furukawa, K. Oh-ishi, M. Nemoto and T. G. Langdon: Proc. Fourth Int. Conf. on 'Recrystallization and related phenomena', (ed. T. Sakai and H. G. Suzuki); 1999, The Japan Institute of Metals, 301–308.
205. Z. Horita, S. Komura, P. B. Berbon, A. Utsunomiya, M. Furukawa, M. Nemoto and T. G. Langdon: *Mater. Sci. Forum*, 1999, **304–306**, 91–96.
206. Z. Horita, S. Lee, S. Ota, K. Neishi and T. G. Langdon: *Mater. Sci. Forum*, 2001, **357–359**, 471–476.
207. Z. Horita, T. Fujinami, K. Sato, S. B. Kang, H. W. Kim and T. G. Langdon: in Proc. James T Staley Honorary Symposium on Aluminum Alloys 'Advances in the metallurgy of aluminum alloys', (ed. M. Tiryakioglu), 271–275; 2001, ASM.
208. P. B. Berbon, S. Komura, A. Utsunomiya, Z. Horita, M. Furukawa, M. Nemoto and T. G. Langdon: *Mater. Trans., JIM*, 1999, **40**, 772–778.
209. M. Nemoto, Z. Horita, M. Furukawa and T. G. Langdon: *Mater. Sci. Forum*, 1999, **304–306**, 59–66.
210. M. Furukawa, Z. Horita, M. Nemeto and T. G. Langdon: Proc. 'Light Metals 1999', Quebec City, PQ, Canada, August 1999, 583–592.
211. M. Furukawa, K. Oh-ishi, S. Komura, A. Yamashita, Z. Horita, M. Nemeto and T. G. Langdon: *Mater. Sci. Forum*, 1999, **304–306**, 97–102.
212. M. Furukawa, A. Utsunomiya, K. Matsubara, Z. Horita and T. G. Langdon: *Acta Mater.*, 2001, **49**, 3829–3838.
213. M. Furukawa, A. Utsunomiya, S. Komura, Z. Horita, M. Nemoto and T. G. Langdon: *Mater. Sci. Forum*, 2001, **357–359**, 431–436.
214. M. Furukawa, Z. Horita and T. G. Langdon: in Proc. James T Staley Honorary Symposium on Aluminum Alloys 'Advances in the metallurgy of aluminum alloys', (ed. M. Tiryakioglu), 47–56; 2001, ASM.
215. M. Furukawa, Z. Horita, M. Nemoto and T. G. Langdon: *Mater. Sci. Eng.*, 2002, **A 324**, 82–89.
216. M. Furukawa, Z. Horita and T. G. Langdon: in 'Ultrafine grained materials II', (ed. Y. T. Zhu, T. G. Langdon, R. S. Mishra, S. L. Semiatin, M. J. Saran and T. C. Lowe), 459–468; 2002, TMS.
217. T. G. Langdon, M. Furukawa, Z. Horita and M. Nemoto: Proc. NATO Advanced Research Workshop on 'Investigations and applications of severe plastic deformation', Moscow, August 1999, NATO Science Series, Series 3, High Technology, vol. 80, Kluwer Academic Publishers, The Netherlands, 2000, 149–154.
218. S. Lee, H. Akamatsu, A. Utsunomiya, K. Neishi, M. Furukawa, Z. Horita and T. G. Langdon: Proc. Thermec 2000, Las Vegas, USA, December 2000.
219. S. Lee, A. Utsunomiya, H. Akamatsu, K. Neishi, M. Furukawa, Z. Horita and T. G. Langdon: *Acta Mater.*, 2002, **50**, 553–564.
220. A. Yamashita, D. Yamaguchi, Z. Horita and T. G. Langdon: *Mater. Sci. Eng.*, 2000, **A 287**, 100–106.
221. K. Oh-ishi, Z. Horita, D. J. Smith and T. G. Langdon: *J. Mater. Res.*, 2001, **16**, 583–589.
222. H. Akamatsu, T. Fujinami, Z. Horita and T. G. Langdon: *Scripta Mater.*, 2001, **44**, 759–764.
223. S. Ota, H. Akamatsu, K. Neishi, M. Furukawa, Z. Horita and T. G. Langdon: *Mater. Trans.*, 2002, **43**, 2364–2369.
224. K. Furuno, H. Akamatsu, K. Oh-ishi, M. Furukawa, Z. Horita and T. G. Langdon: *Acta Mater.*, 2004, **52**, 2497–2507.
225. I. N. Fridlyander, O. G. Senatorova, N. A. Ryazanova and A. O. Nikiforov: *Mater. Sci. Forum*, 1994, **170–172**, 345–349.
226. J. N. Fridlyander and O. G. Senatorova: *Mater. Sci. Forum*, 1996, **217–222**, 1813–1818.
227. J. Liu and D. J. Chakrabarti: *Acta Mater.*, 1996, **44**, 4647–4661.
228. O. G. Senatorova, A. N. Uksusnikov, J. N. Fridlyander, J. Koshorst, R. R. Romanova, N. A. Ryazanova, A. Galliot and V. V. Cherkassov: Proc. 6th Int. Conf. on 'Aluminum alloys', July 1998, Toyohashi, Japan, 589–593.
229. R. A. Emigh, E. L. Bradley and J. W. Morris, Jr: in 'Superplasticity in aerospace II', (ed. T. R. McNelley and H. C. Heikkenen), 303–315; 1990, TMS.
230. E. L. Bradley, III, R. A. Emigh and J. W. Morris, Jr: *Scripta Metall. Mater.*, 1991, **25**, 717–721.
231. N. I. Kolobnev, L. B. Khokhlatova, V. D. Makarov, E. Yu. Semenova and V. V. Redchits: Proc. Sixth Int. Aluminium–Lithium Conference, Garmisch-Partenkirchen, Germany, October 1991, 1053–1056.
232. N. K. Tsenev, R. Z. Valiev, O. V. Obraztsov and I. N. Fridlander: Proc. Sixth Int. Aluminium–Lithium Conference, Garmisch-Partenkirchen, Germany, October 1991, 1125–1132.
233. A. M. Shammazov, N. K. Tsenev, R. Z. Valiev, M. M. Myshlyaev, M. M. Bikbulatov and S. P. Lebedich: *Phys. Met. Metall.*, 2000, **89**, (3), 314–318.
234. F. Musin, R. Kaibyshev, Y. Motohashi, T. Sakuma and G. Itoh: *Mater. Trans. A*, 2002, **43A**, 2370–2377.
235. M. Shagiev, Y. Motohashi, F. Musin, R. Kaibyshev and G. Itoh: *Mater. Trans. A*, 2003, **44A**, 1694–1697.
236. M. Shagiev, Y. Motohashi, F. Musin, R. Kaibyshev and G. Itoh: *Mater. Trans. A*, 2003, **44A**, 1698–1701.
237. B. A. Parker and Z. F. Zhou: Proc. 3rd Int. Conf. on 'Aluminium alloys', Vol. I, NTH, Trondheim, Norway, June 1992, 363–367.
238. J. R. Davies: 'ASM specialty handbook: aluminum and aluminum alloys'; 1993, Materials Park, OH, USA, ASM.
239. S. J. Andersen, H. W. Zandbergen, J. Jansen, C. Traeholt, U. Tundal and O. Reiso: *Acta Mater.*, 1998, **46**, 3283–3298.
240. M. L. Kharakterova, D. G. Eskin and L. L. Rokhlin: *Russ. Metall.*, 1997, (1), 104–109.
241. J. Røyset: Dr. Ing. thesis, NTNU, Trondheim, Norway, 2002.
242. P. P. Chattopadhyay, S. Datta and M. K. Banerjee: *Mater. Sci. Eng.*, 2002, **A 333**, 67–71.
243. L. I. Kaigorodova, E. I. Selnikhina, E. A. Tkachenko and O. G. Senatorova: *Phys. Met. Metall.*, 1996, **81**, 513–519.
244. Y.-L. Wu, F. H. Froes, C. Li and A. Alvarez: *Metall. Mater. Trans. A*, 1999, **30A**, 1017–1024.
245. Z. Yin, L. Yang, Q. Pan and F. Jiang: *Trans. Nonferrous Met. Soc. China*, 2001, **11**, 822–825.
246. V. I. Elagin, V. V. Zakharov and T. D. Rostova: *Met. Sci. Heat Treat.*, 1994, **36**, (7), 375–380.
247. Y. V. Milman, A. I. Sirko, D. V. Lotsko, O. N. Senkov and D. B. Miracle: *Mater. Sci. Forum*, 2002, **396–402**, 1217–1222.
248. C.-H. Joh, K. Yamada and Y. Miura: *Mater. Trans., JIM*, 1999, **40**, 439–442.
249. X. J. Jiang, Q. H. Gui, Y. Y. Li, L. M. Ma, G. J. Liang and C. X. Shi: *Scr. Metall. Mater.*, 1993, **29**, 211–216.
250. X. J. Jiang, Y. Y. Li, W. Deng, L. Y. Xiong, W. M. Wu, Y. J. Gao and C. X. Shi: *Adv. Cryogenic Eng. (Mater.)*, 1994, **40**, 1369–1376.
251. C.-H. Joh, T. Katsube, K. Yamada and Y. Miura: Proc 6th Int. Conf. on 'Aluminum alloys', Toyohashi, Japan, July 1998, 799–804.
252. L. I. Kaygorodova, A. M. Dritz, T. V. Krymova and I. N. Fridlyander: Proc. Sixth Int. Aluminium–Lithium Conference, Garmisch-Partenkirchen, Germany, October 1991, 363–367.
253. L. I. Kaigorodova, A. M. Drits, Ya. V. Zhingel, T. V. Krymova and I. N. Fridlyander: *Phys. Met. Metall.*, 1992, **73**, 286–290.
254. A. L. Berezina, V. A. Volkov, S. V. Ivanov, N. I. Kolobnev and K. V. Chuistov: *Phys. Met. Metall.*, 1991, **71**, (2), 167–175.
255. I. N. Fridlyander, N. I. Kolobnev, A. L. Berezina and K. V. Chuistov: Proc. Sixth Int. Aluminium–Lithium Conference, Garmisch-Partenkirchen, Germany, October 1991, 107–112.
256. L. I. Kaigorodova, A. M. Drits, Ya. V. Zhingel, T. V. Krymova and V. A. Rassokhin: *Phys. Met. Metall.*, 1992, **73**, 281–285.
257. I. N. Fridlyander, S. F. Danilov, E. N. Malysheva, T. A. Gorokhova and N. N. Kirkina: Proc. Sixth Int. Aluminium–Lithium Conference, Garmisch-Partenkirchen, Germany, October 1991, 381–386.
258. G. Dlubek, S. Krause, H. Krause, A. L. Beresina, V. S. Mikhalenkov and K. V. Chuistov: *J. Phys. Condens. Matter*, 1992, **4**, 6317–6328.
259. S. Krause, H. Krause, G. Dlubek, A. L. Beresina and K. S. Chuistov: *Mater. Sci. Forum*, 1992, **105–110**, 1109–1112.
260. C. Y. Tan, Z. Q. Zheng and S. Q. Liang: Proc. 4th Int. Conf. on 'Aluminium alloys', Vol. II, Atlanta, GA, USA, September 1994, 329–333.
261. A. L. Beresina, N. I. Kolobnev, K. V. Chuistov, A. V. Kotko and O. A. Molebny: *Mater. Sci. Forum*, 2002, **396–402**, 977–981.

262. I. N. Ganiev, I. Yunusov and V. V. Krasnoyarskii: *J. Appl. Chem. USSR*, 1986, **60**, 1961–1965.
263. I. N. Ganiev: *Prot. Met.*, 1995, **31**, 543–546.
264. N. V. Vyazovikina: *Prot. Met.*, 1999, **35**, 448–453.
265. G. V. Kharina and V. P. Kochergin: *Prot. Met.*, 1996, **32**, 134–136.
266. G. V. Kharina, M. V. Kuznetsov and V. P. Kochergin: *Russ. J. Electrochem.*, 1998, **34**, 482–485.
267. V. S. Sinyavskii, V. D. Val'kov and E. V. Titkova: *Prot. Met.*, 1998, **34**, 549–555.
268. Y. L. Wu, F. H. Froes, C. G. Li and J. Liu: Proc. 'Synthesis/processing of lightweight metallic materials II', Orlando, FL, USA, February 1997, 73–81.
269. Z. Ahmad and B. J. Abdul-Aleem: Proc. EuroCorr 2000.
270. Z. Ahmad, A. Ul-Hamid and B. J. Abdul-Aleem: *Corros. Sci.*, 2001, **43**, 1227–1243.
271. R. Braun, B. Lenczowski and G. Tempus: *Mater. Sci. Forum*, 2000, **331–337**, 1647–1652.
272. T. Torma, E. Kovács-Csetényi, L. Vitális, I. Vitányi, J. Stepanov and M. Butova: *Mater. Sci. Forum*, 1987, **13/14**, 497–503.
273. Z. Wang, P. Wang, K. S. Kumar and C. L. Briant: in 'Chemistry and electrochemistry of corrosion and stress corrosion cracking', (ed. R. H. Jones), 573–582; 2001, TMS.
274. V. I. Elagin, V. V. Zakharov, A. A. Petrova and E. V. Vyshegorodtseva: *Russ. Metall.*, 1983 (4), 143–146.